University of Liège: Master Thesis

Optimisation of the Energy Harvesting and Management Systems of the Nanosatellite OUFTI-2 and Design of its Electrical Power Supply

By

François Grosjean

Department of Electrical Engineering
University of Liège

A thesis submitted to the University of Liège in accordance
with the requirements of the degree of
Master in Electrical Engineering
in the Faculty of Applied Sciences.

June 2019

Supervisor : Philippe Vanderbemden

Abstract

The aim of this thesis is to design a part of the Electrical Power Supply (EPS) board of the nanosatellite OUFTI-2.
The parameters to be fixed are the solar panels' configuration and management, the Battery Management System (BMS), and their connection to the DC-DC converters distributing the power to all sub-systems.

The battery pack, the solar panels and the DC-DC converters are already chosen from previous works on the satellite. The limitations and requirements imposed by the choice of these components are analysed. The state of the art of Maximum Power Point Tracking (MPPT) technology as well as Battery Management Systems (BMS) of Lithium-Polymer (LiPo) are summarised and compared.

From this knowledge, several relevant EPS designs combining different MPPT controllers and BMS configurations are discussed and tested as well as their power paths.

The final design is chosen to be a semi-regulated bus connecting two SPV1040 MPPT controllers in series and a MCP73213 linear BCR to the DC-DC converters.

Finally, the power budget of the satellite's consumption and harvested power, based on the final architecture design, is discussed on a worst case scenario. This analysis ensures the EPS to supply the satellite, its payload and the charge of the battery.

Keywords

OUFTI-2, CubeSat, D-STAR, Electrical Power Supply, Maximum Power Point Tracking, Battery Charger, Semi-regulated Bus, Power Path, Power budget

Dedication and acknowledgements

The completion of this thesis could not have been possible without the help and contribution of several people.
I would like to specifically express my gratitude to:

Mr Jacques Verly, Mr Valery Broun and Mr Sebastien De Dijcker for proposing me this thesis.

The whole OUFTI team and especially Mr Sylvain Guichaux for their help and sympathy during this work.

Mr Philippe Vanderbemden for his pieces of advice and his proof readings along the redaction of the thesis.

My relatives and my girlfriend for their endless support and motivation.

Mss Elizabeth Cook for her excellent proof readings and all the pertinent remarks.

Mss Emilie Grosjean for her help with the layout of the thesis.

A special thank to Mr Valery Broun who advised me throughout the thesis.

I finally would like to warmly thank Mr Verly and Mr Broun for giving me the opportunity to present the satellite and my work in Malaga for the SSSIF event.

Herstal, June 6, 2019.

List of acronyms

1U	One Unit of a CubeSat
2s1p	Battery configuration of two cells in series and one cell in parallel
ADC	Analog-to-Digital Converter
BCN	Beacon
BCR	Battery Charger
BoL	Beginning of Life
CAD	Computer-Aided Design
CC/CV	Constant Current, Constant Voltage
CV	Constant Voltage
DET	Direct Energy Transfer
DoD	Depth of Discharge
DPC	Dual Processor Core
EoL	End of Life
EPS	Electrical Power Supply
IC	Incremental Conductance
IMU	Inertial & Magnetic Measurement Unit
ISS	International Space Station
I-V	Current versus Voltage
MPP	Maximum Power Point
MPPT	Maximum Power Point Tracking
PCB	Printed Card Board
SA	Solar Array
OBC	On Board Computer
OUFTI	Orbital Utility For Telecommunication Innovation
PID	Proportional-Integral-Derivative controller
P&O	Perturb & Observe
P-V	Power versus Voltage
RAD	Radiation
Rx	Receive

STK Systems Tool Kit
Tx Transmission
UHF Ultra High Frequency
UTJ Ultra Triple Junction
VHF Very High Frequency

Table of Contents

List of Tables

List of Figures

Figure **Page**

1 Introduction

Energy is a challenge in space, especially for a low power mission such as the nanosatellite OUFTI-2.
The Electrical Power System (EPS) is the power factory of the satellite. It is responsible for harvesting, managing and distributing the power around the spacecraft in the safest and most efficient way. A critical attention must be paid to its design, as a failure would lead to the end of the mission.

In the case of OUFTI-2, as for many Low Earth Orbit (LEO) missions, solar arrays are used as the first energy source. A battery pack, as second energy source, powers the satellite during eclipses.

The power distribution, which is the final part of the EPS, has already been determined by Valery Broun. Four DC-DC buck converters are used to supply all the sub-systems of the satellite with 4 different regulated voltages:

- 5V to drive the beacon
- 3.3V at high current to drive the transmission communications
- 3.3V at low current to drive the on board computer and all other sub-systems
- 1.8V to drive the on board computer

These converters are powered either powered by the solar panels or by the batteries during eclipses.

In addition to these DC-DC converters, the EPS board hosts four analog to digital converters (ADC). Their goal is to measure the voltages, currents and temperature of the board. Two ADC are used by the Beacon (BCN) which emits these data; the other two ADC are connected to the On Board Computer (OBC) to monitor the state of the EPS.

The goal of this thesis is to finalise the design of the EPS of OUFTI-2: the power control and power harvest section. The main challenge is to combine the requirements of the batteries and the solar arrays into an efficient and reliable design for the satellite.

2 The OUFTI project

2.1 CubeSat concept

A CubeSat is a small square-shaped, cost-effective nanosatellite. A CubeSat unit (1U) has a standard dimension of $10cm^3$ and must weight less than 1.33kg [1]. The modularity of the satellite allows several small units to be combined in order to form a larger structure.
The concept emerged from two professors from the California Polytechnic State University and the Stanford University in 1999. Their aim is to provide a low-cost satellite concept for companies and universities to facilitate the access to space applications.
Nowadays, several universities have been working to launch their own CubeSats, offering the opportunity for students to get hands-on experience with the design and operation of a satellite.

2.2 OUFTI-1 background

OUFTI-1 uses the CubeSat concept. It comes from an initiative started in September 2007 by the University of Liège and the Higher Education Institution of the Province of Liège[2]. It is a 1U designed and built by students of the two institutes. It is the first nanosatellite ever developed in Belgium.

The acronym of the satellite stands for `Orbiting Utility For Telecommunication Innovation`. It also is a typical interjection from the city of Liège.
OUFTI-1 is the first nanosatellite ever developed in Belgium. OUFTI-1 was selected to be part of the "Fly your satellite" project organised by the European Space Agency (ESA). This project offered a flight opportunity on the Vega maiden flight for several CubeSats.
The nanosatellite was launched alongside three other CubeSats from Kourou space centre on April 25, 2016.

The payload, the main mission of the project, is to operate a D-STAR digital communication protocol repeater into orbit.

2.2.1 D-STAR protocol

The D-STAR protocol, which stands for Digital Smart Technology for Amateur Radio, is a ham radio protocol developed by the Japan Amateur Radio League[3]. The system provides a digital communication, simultaneous voice and data transmissions and a routing to the internet.
The University of Liège is equipped with a repeater that is uses to connect to the orbital repeater.

2.2.2 Orbital operation

After a successful launch on 25 April 2016, OUFTI-1 reached its orbit as planned.
However, an unknown failure caused a malfunction of the satellite and communications cannot be established with the CubeSat.
Luckily, as the beacon was designed in parallel from the OBC, some parameters of the satellite were successfully transmitted to ground for a few days.

One of the reasons suspected to be the cause of the failure is radiation.
The apogee of the orbit is at 1447km[3], located in the inner Van Allen belt. This radiation belt is located between 1000km to 6000km from Earth's ground. A high concentration of high energy particles is trapped in this region due to the Earth's magnetic field.
Figure 2.1 depicts the situation[4].

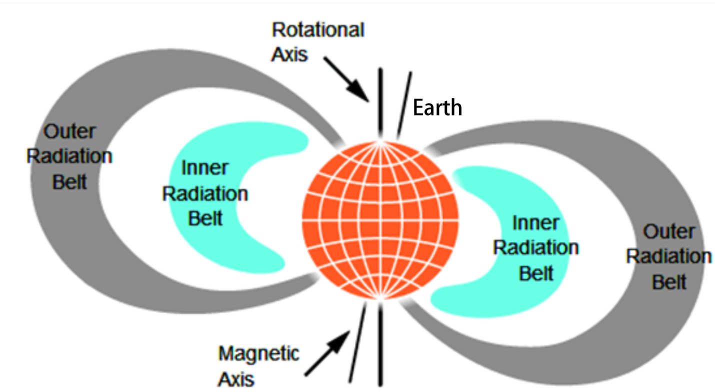

Figure 2.1: Representation of the inner and outer Van Allen belt

At the time of writing (June 2019),OUFTI-1 is still orbiting the Earth, and can be tracked via: `https://www.n2yo.com/satellite/?s=41458#results`.

2.2.3 OUFTI-1 EPS

The goal of the EPS of OUFTI-1 was to connect the 10 high-efficiency `AZURSPACE` solar cells to two Lithium Polymer (LiPo) battery cells in parallel through an unregulated bus. Both the batteries and the solar cells are then connected to three DC/DC converters able to power the rest of the circuit with DC voltages of 5V, 3.3V and 7.2V.
Figure 2.2, from the thesis of Pierre Thirion, shows the high-level architecture of the board.[5]

From his power analysis, Thirion decided not to use the Maximum Power Point Tracking (MPPT) technology in the architecture of the EPS of OUFTI-1.
The solar cells are placed onto 5 sides of the cube, the last one being reserved for antennas and

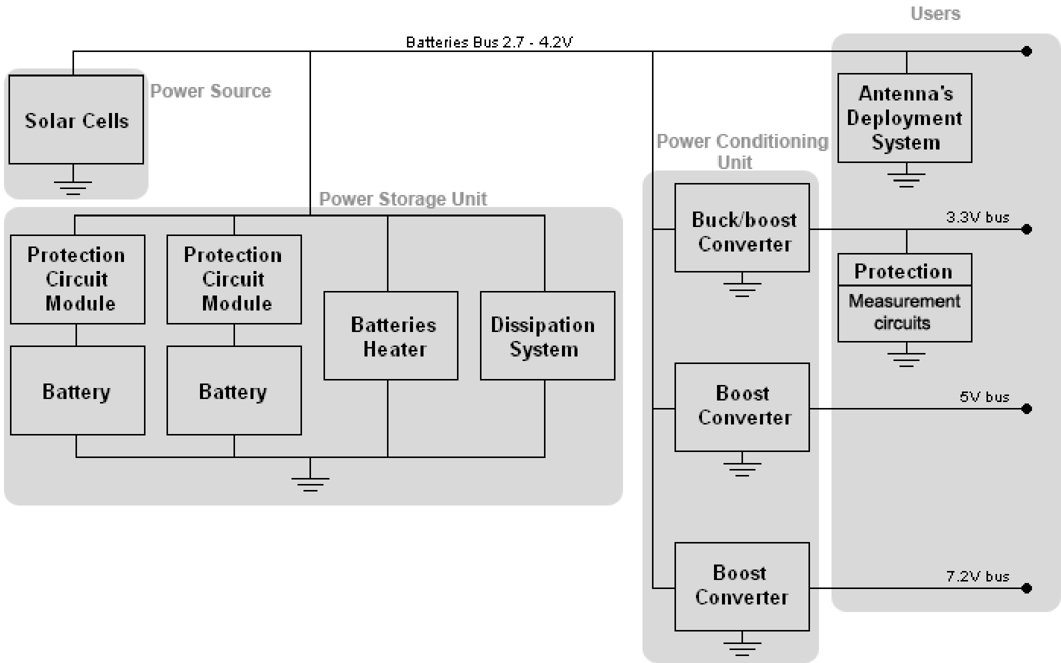

Figure 2.2: High-level architecture of the EPS of OUFTI-1

their deployment system. Two cells per side are connected in series, and each side is connected in parallel to the unregulated voltage bus varying between 2.7V and 4.2V.
As the voltage of a LiPo battery cell is around 4V, this causes no problem with directly connecting the solar cells to the battery. Some protection features such as overvoltage, undervoltage, overcurrent and temperature regulation are set up.

This architecture cannot be used in OUFTI-2 for several reasons which are explained in the next section.

2.3 OUFTI-2

2.3.1 Mission goals

After the communication loss of OUFTI-1, the learnings needed to be applied to a new version of the satellite. The OUFTI-2 project was born.

OUFTI-2 shares some similar characteristics with OUFTI-1 in its mechanical structure and in its main payload, i.e. the D-STAR protocol.
However, some major changes are made inside the CubeSat due to both internal and external factors. As the deployment will be operated from the International Space Station (ISS), some additional securities must be ensured for manned flight.
Furthermore, secondary payloads are added to the system.

- A radiation board testing two different types of electronics shielding from space ionising radiation
- An inertial & magnetic measurement unit (IMU) which estimates the attitude of the satellite
- A new Dual Processor Core (DPC)

This new DPC from Thales Alenia Space is of interest to this thesis since it consumes a significant amount of power.
The DPC has been introduced to prevent the OBC from undergoing single event latch-up due to space radiation, what is thought to be the cause of failure of OUFTI-1.
As the chip is still in development, OUFTI-2 constitutes its first flight test.

2.3.2 Sub-systems

This section introduces all the sub-systems of OUFTI-2, in order to understand the different consumption of the satellite (cfr. Chapter 10.1).

Figure 2.3 represents an exploded view of OUFTI-2 and its sub-systems designed by the OUFTI team. The satellite is made of six boards stacked one above the other, connected through PC104 connectors.

The first board is the Beacon (BCN), which emits essential parameters of the satellite in Morse code, at a rate of 12 words per minute.
The beacon intersperses the emission with bursts of all the data at 2400 bauds, an additional feature compared to OUFTI-1. The two rates have different consumptions and activation times.

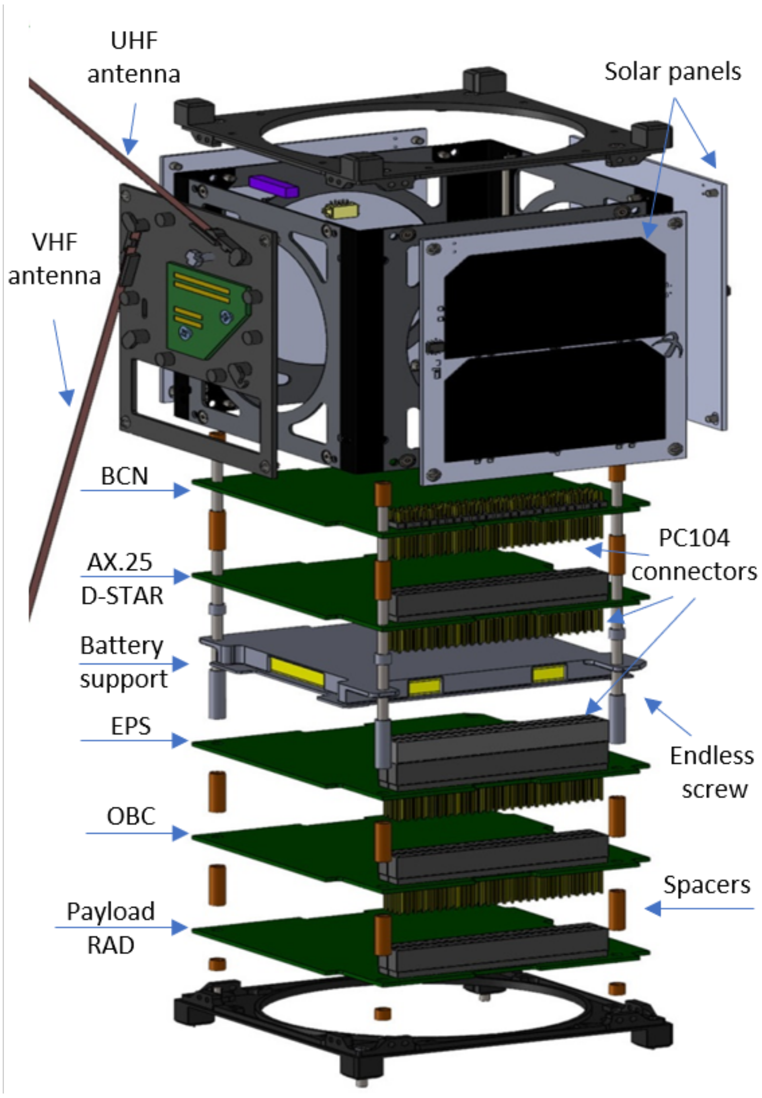

Figure 2.3: Exploded view of OUFTI-2 and its sub-systems

The next board is the communication board, hosting the D-STAR and the AX.25. The two data protocols share a Very High Frequency (VHF) and an Ultra High Frequency (UHF) antennas to communicate with the ground.
Both communication protocols have receiver (Rx) and transmission (Tx) modes. As the antennas have to be shared, only one protocol can transmit at a time.

The third board is the battery pack, explained in section 2.3.3.2. It is followed by the fourth board, the EPS, subject of this thesis.
The OBC has its own board as well. The secondary payloads IMU and RAD are placed on the last board.

As for OUFTI-1, the satellite does not require high-precision orientation for its communications. A passive magnetic attitude stabilisation control is therefore best fitted for the application. Magnets in the z axis of the satellite forces the CubeSat to align with the Earth's magnetic field, limiting its spin. Figure 2.4, from a former thesis [6] about OUFTI's passive attitude control, represents the situation.

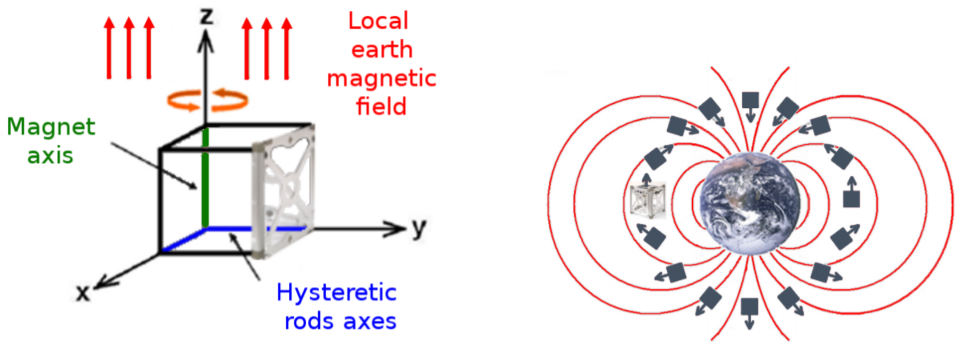

Figure 2.4: Passive magnetic attitude stabilisation control for OUFTI-2

The importance of this passive control is explained in chapter 5.

2.3.3 State of the electrical power supply system of OUFTI-2

A part of the EPS has already been determined before this thesis and the solar cells and battery pack have already been chosen.
The new solar cells and batteries constitute an important change from OUFTI-1 and are requirements for the design of the EPS of OUFTI-2. They are described below.

2.3.3.1 SpectroLab Solar Cells

For OUFTI-2, the Azurspace solar arrays used on OUFTI-1 are replaced by Ultra Triple Junctions (UTJ) from Spetrolab. The main electrical characteristics of a 26.62 cm^2 UTJ cell are summarised in Table 2.1.[7].

The maximum power produced by one cell in these conditions is then:

$$P = J_{MP} * V_{MP} * A = 1019\text{mW} \tag{2.1}$$

where A is the area of the cell.

Each solar panel mounted on OUFTI-2 is made out of two of these 26.62 cm^2 cells connected in series. Each side of the cube is equipped with one solar panel, except for one side, reserved

Short-Circuit Current Density, J_{SC} [mA/cm^2]	17.05
Maximum Power Current Density, J_{MP} [mA/cm^2]	16.30
Open Circuit Voltage, V_{OC} [V]	2.66
Maximum Power Voltage, V_{MP}[V]	2.35
Maximum Power Efficiency at Beginning Of Life (BOL), η_{MP} [%]	28.3

Table 2.1: Electrical characteristics of a 26.62cm^2, Ultra Triple Junction (UTJ) Spectrolab solar cell under 135.3mW/cm^2 illumination and at 28°C

for the antennas and their deployment system.

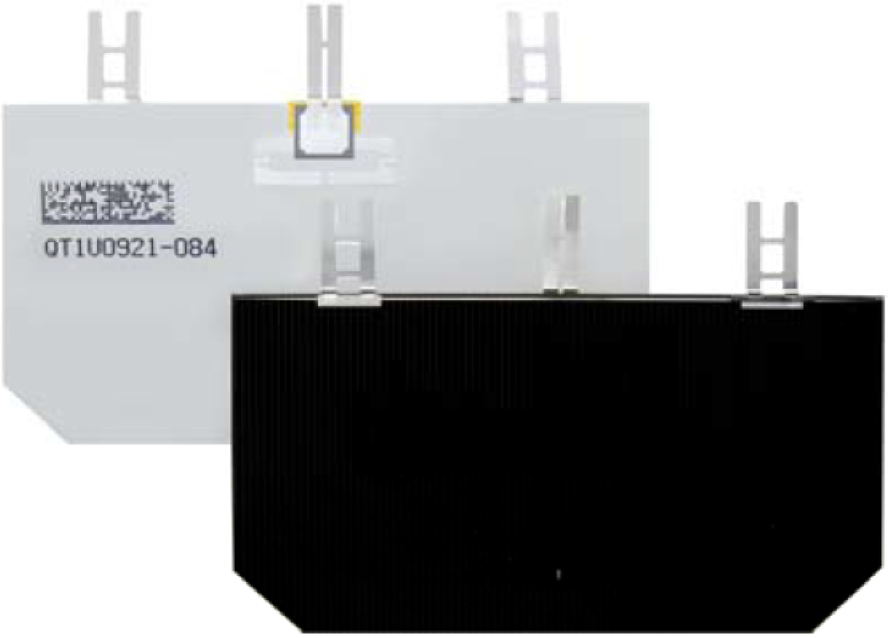

Figure 2.5: Representation of the 26.62cm^2, ultra triple junction Spectrolab solar cell

2.3.3.2 ClydeSpace batteries

An important change from OUFTI-1 is the International Space Station (ISS) deployment. The satellite is launched to the ISS where the CubeSat is deployed in orbit. This new deployment has the advantage of being much cheaper while still enabling the test of the payload.
However, to protect the ISS and the astronauts inside of it, more constraints are imposed on the CubeSat, such as manned-flight batteries. The previous batteries used in OUFTI-1 were not conceived for such conditions and had to be replaced by 10Wh standalone Lithium-Polymer (LiPo) batteries from ClydeSpace, a Boeing company.

Compared to OUFTI-1, the new battery cells are now connected in series (2sp1), which forces an entirely new design of the EPS.

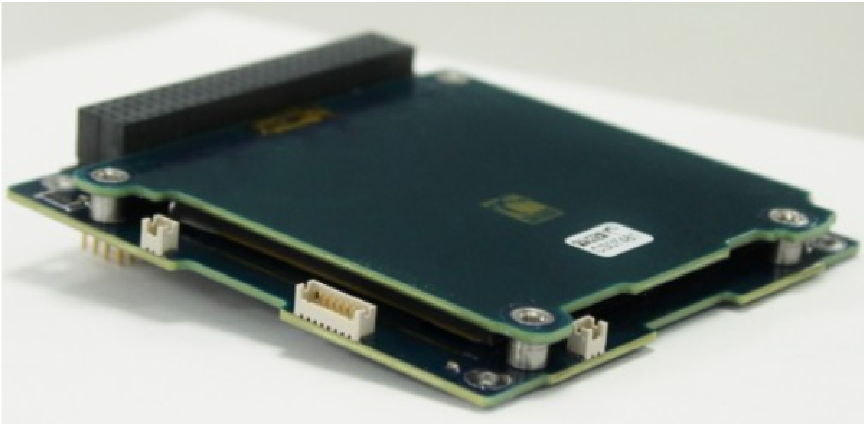

Figure 2.6: Representation of the 10Whr ClydeSpace batteries used on OUFTI-2

This high energy density battery pack presents these characteristics[8]:

- Nominal Capacity of 1,3Ah in the range 6-8.4V
- PC104 format compatible for CubeSat [9]
- Compatible with ISS Manned Flight design requirements
- Battery protection such as overcharge, overdischarge, overcurrent and overvoltage
- Integrated heater preventing the batteries temperature from dropping below 1°C

3 Solar cell management in OUFTI-2

Energy is a challenge for every space application. From the power budget in chapter 10, the mean power consumption of OUFTI-2 reaches 1231mW without transmission, i.e. nearly 30% more power than OUFTI-1 [5].
This is essentially due to the high consumption of the new dual core processor. The consumption of the OBC has risen from 25mW, for OUFTI-1, to 458mW for OUFTI-2, as can be seen in appendix 13.
Efficient power management and harvesting systems are therefore essential.

3.1 Solar cells

Solar Arrays (SA) for satellite are somewhat different to ground SA. Although the principle stays the same, the environment encountered and the insolation scenarios are different.
The goal of this section is to understand a solar cell in order to simulate the behaviour of the `Spectrolab UTJ` solar cells used on OUFTI-2.

3.1.1 Theoretical approach

A solar cell is a semiconductor device which uses the photovoltaic effect to convert the solar energy into electrical energy. A solar cell is typically made of a large silicon substrate with two neutral doped regions, an N-side with an excess of free electrons, and a P-side with an excess of free holes. A hole is an absence of electron.
At the junction of the doped regions, the excess carriers of each side diffuse to the other region. After crossing it, the carriers recombine and cancel out near the junction. Hence, near the junction, positive ions are left in the N-side, and negative ions on the P-side. An internal electric field is induced in this region, called the depletion region.

When photons with energies higher than the substrate's energy band gap penetrate to the depletion region, a mobile electron-hole pair is generated. The mobile charge are then carried away by the electric field. As the number of high energy photons increases, so does the density of mobile electron-hole pairs. These moving charges are the so called photogenerated current, I_L.

An internal representation of this principle is shown in Figure 3.1. E_g and E_p are respectively the band gap energy of the substrate and the energy of the incoming photon.

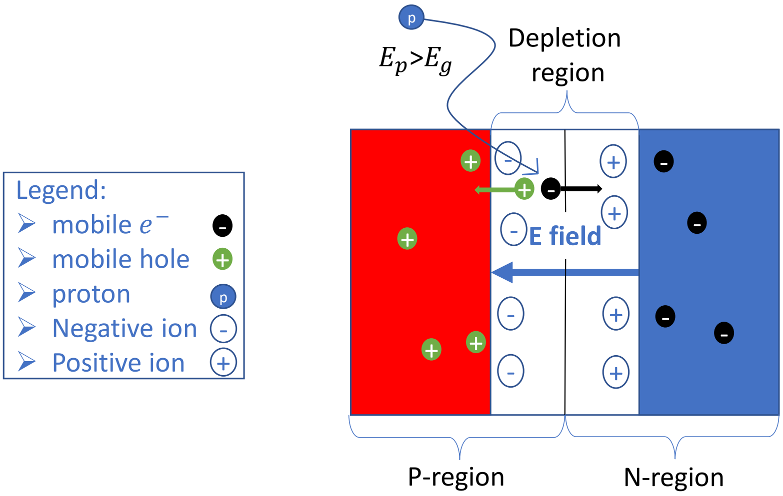

Figure 3.1: Internal representation of a typical solar cell

Figure 3.2, from [10], shows a simple electric model of a solar cell when perfect are components assumed.

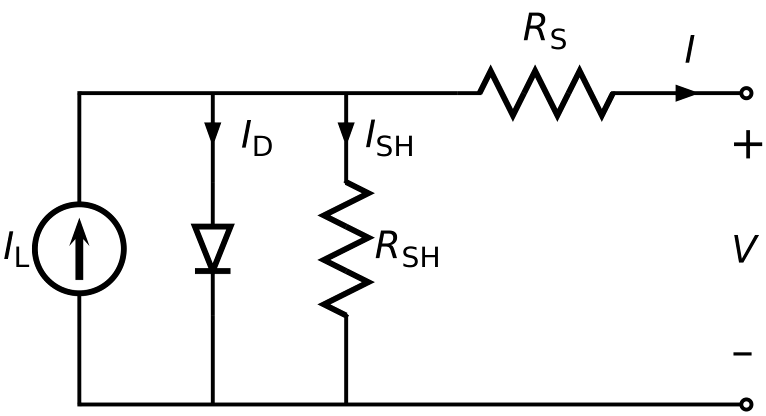

Figure 3.2: Solar cell equivalent circuit model

From the photogenerated current, a solar cell can be considered as a current injector in parallel with a diode. As the cell is not perfect, a series and shunt resistors, respectively R_S and R_{SH} are added in order to model the losses [10].
The current produced by the cell, I, can then be expressed as:

$$I = I_L - I_D - I_{SH} \tag{3.1}$$

where I_L is the photogenerated current, I_D, the current going through the diode, and I_{SH}, the current through the shunt resistor.

From the Shockley diode equation, the current flowing through a diode is function of the voltage at its terminals, V_D:

$$I_D = I_0 \left(e^{\frac{V_D}{nV_T}} - 1\right) \tag{3.2}$$

where:

- I_0 is the reverse saturation current
- V_T is the thermal voltage, which is nearly 25mV at 28 °C
- n is the quality factor of the junction (> 1)

The voltage across the diode can be determined through the model and from Ohm's law:

$$V_D = V + IR_S \tag{3.3}$$

Therefore, from equations 3.1, 3.2 and 3.3, the output current produced by the cell can be expressed as:

$$I = I_L * I_0 \left(e^{\frac{V+IR_S}{nV_T}} - 1\right) - \frac{V+IR_S}{R_{SH}} \tag{3.4}$$

For a specific cell, the knowledge of R_S, R_{SH}, I_L and I_0, allows its characteristic current versus voltage (I-V) curve to be drawn.
Obviously, the photogenerated current, I_L, depends on the insolation while the thermal voltage, V_T, depends on the temperature of the cell.

For a specific I-V curve, the operating point of the solar cell is a certain current voltage pair. An operating point can be located at any point of the I-V curve of the cell.

3.1.2 Simulation of OUFTI-2's solar cells

Through equation 3.4 a matlab script can be implemented to compute the output current of a cell for which the model is known, for a specific output voltage, insolation and temperature. This script, called `CellUTJ.m`, was first written by the CubeSat team of SwissCube and has been improved and adapted to the solar cells of OUFTI-2.

Two additional scripts have also been created through the work of this thesis.
The first one, `plotCell.m`, plots the I-V curve and the power versus voltage (P-V) curve of two OUFTI-2's solar cells in series for a given insolation and temperature.
The second one, `load2.m`, plots the I-V curve of one of OUFTI-2's solar panel.
The scripts are presented in the appendix 13.

Figure 3.3, plotted with `plotCell.m`, shows the I-V and P-V curves of one of OUFTI-2's solar panel, at 28 °C and under an illumination of 1367W/m^2, a typical solar constant. To simplify the script, relative insolation, G was introduced, where G=1 corresponds to an insolation of 1367W/m^2.

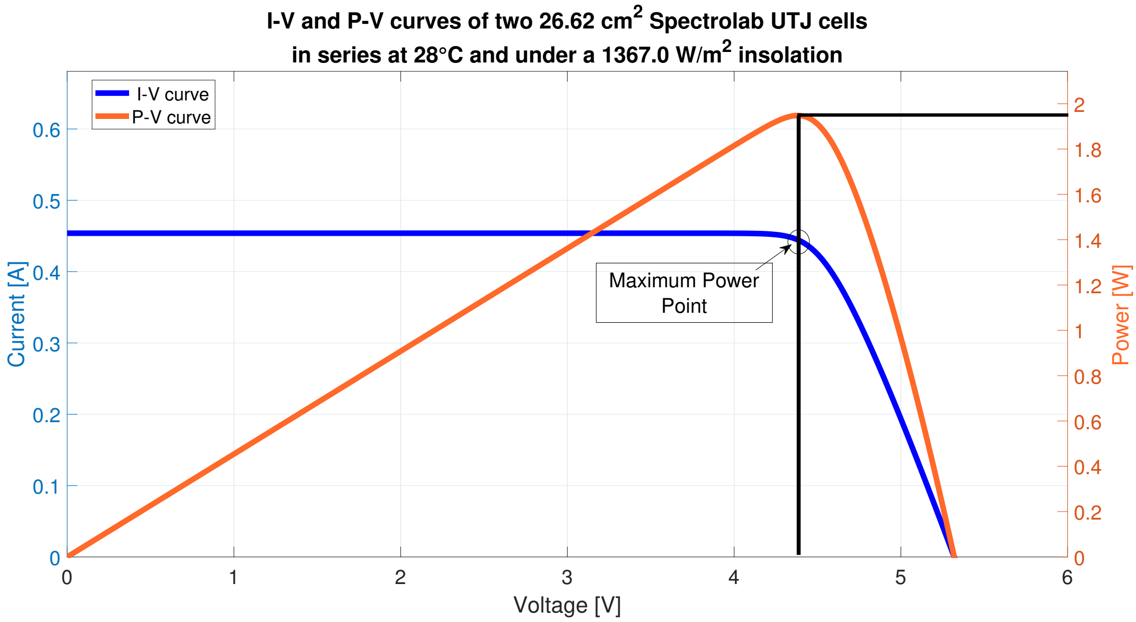

Figure 3.3: Current vs voltage curve and power vs voltage curve of one 26.62 cm^2 `Spectrolab` cell under an irradiance of 1367W/m^2 at 28 °C

Figure 3.4, plotted with `load2.m`, shows the I-V curve of the `Spectrolab` solar cell of OUFTI-2, at 28 °C and under a relative insolation G of 1. Three different loads, R, of 1Ω, 5Ω and 10Ω, are also plotted.
The operating point of the cell corresponds to the I-V point the solar cell is operating at right now. This point is always located at the intersection of the I-V curves of the solar cell and the load.

Figure 3.3 shows that it exists a point where the cell outputs the maximum power known as the maximum power point (MPP).
It can be seen that the MPP of the panel is located at 4.3V and that the power produced if the panel operates at this point is 1950mW.
These values correspond to the characteristics of the `spectrolab` solar cell that were presented in Table 2.1.

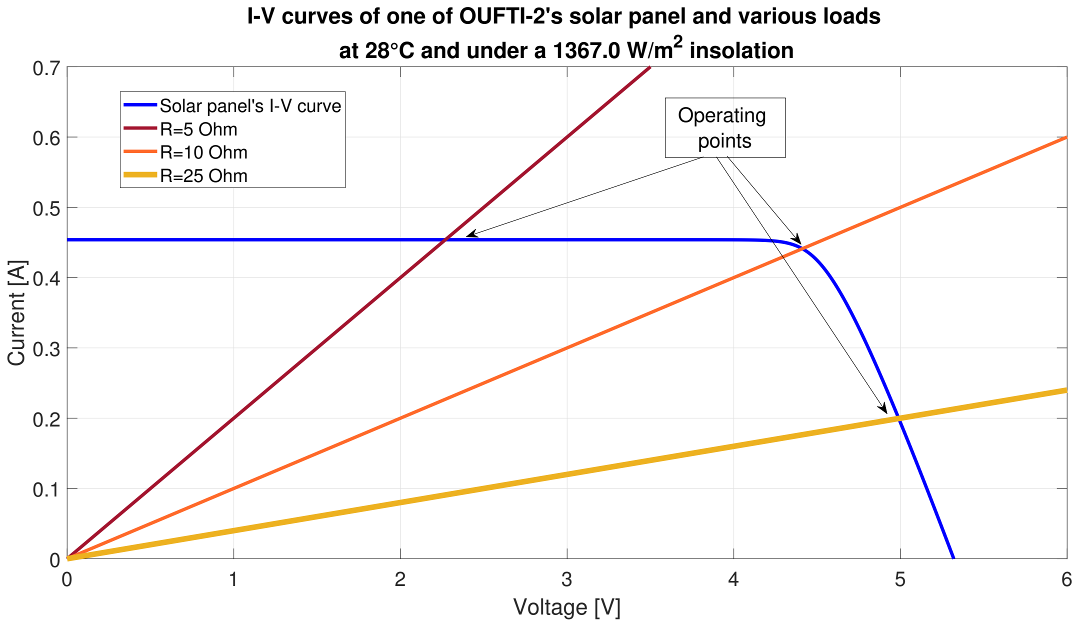

Figure 3.4: Current vs voltage curve of the 26.62 cm^2 `Spectrolab` cell under an irradiance of 1367W/m^2 at 28 °C intersected by 3 different loads of 1Ω, 5Ω and 10Ω

However, as the I-V curve of a solar cell varies with temperature and sun irradiation, so does its MPP. It is then crucial to be able to vary the load to always operate the cell at the MPP. These variations were simulated with one of OUFTI-2's solar panel.

(a)

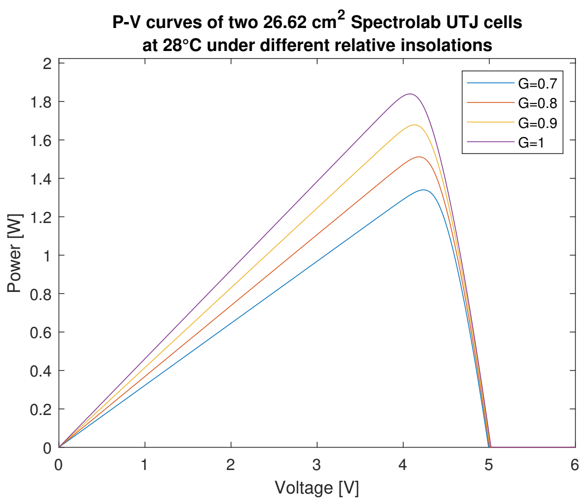

(b)

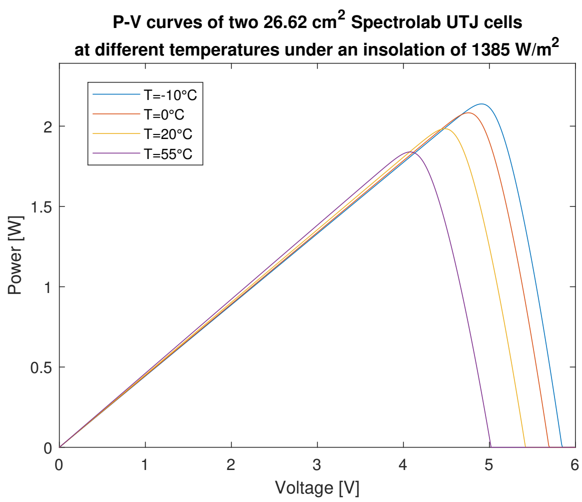

Figure 3.5: (a) Power-Voltage curve of two 26.62 cm^2 `Spectrolab` cells under relative insolations, G, of 1,0.9,0.8 and 0.7, at 28 °C, (b) Power- Voltage curve of two 26.62 cm^2 `Spectrolab` cells under an irradiance of 1385W/m^2 at -10°C, 0°C, 20°C and 55 °C

The changes of MPP position under different insolations and temperatures of the cells are represented in Figures 3.5(a) and 3.5(b). These plots are obtained through the matlab scripts `plotCellsG.m` and `plotCellsT.m` that can be found in appendix 13.

From both Figures 3.5(a) and 3.5(b), the voltage of maximum power of the solar panel, V_{MPP}, is confined between 4.2V to 5.2V.
The minimum V_{MPP} a panel of OUFTI-2 can operate at is found for a maximum insolation and temperature, i.e G=1 and T=100°, the maximum temperature supported by the cell. This V_{MPP} is equal to 3.62V and corresponds to a power of 1629mW. These results are found through the matlab script `plotCellsT.m` in the appendix 13.

A MPP tracking (MPPT) algorithm can then be implemented to adjust the load of the solar cell as its IV curve changes. Chapter 4 discusses several MPPT algorithms.

3.1.3 Solar panels configuration

For OUFTI-2, the 5 sides of the cube are equipped with two solar cells in series, each side forming a solar panel. This section analyses the series and parallel connection of two OUFTI2's solar panels.

Under the same temperature and insolation conditions, two panels have the same I-V curve and operate at the same operating point.
In a series topology, the output voltage is simply doubled for the same current. Hence, the total power is doubled.

If the solar cells have different insolation, the current is limited by the less conductive panel, i.e. the less illuminated one. If only one panel is totally shaded, this leads to no current through both.

In a parallel configuration, the voltage of both panels is fixed while their generated current are added. Under different insolations, the solar panels have different I-V curves. Hence, for a same voltage, they produce different currents. If a panel is totally shaded, it produces no current, but the other panel is still conductive. An anti-reverse current diode preventing the current from one panel from flowing into the shaded one is therefore needed.

As the solar panels of OUFTI-2 have different orientations, the series configuration is extremely inefficient. Hence, the panels can only be connected in parallel, with one anti-reverse current diode per panel.

However, as mentioned in the introduction, the battery pack has a nominal voltage of 7.4V. As the panels cannot be placed in series, another method must be investigated in order to boost the voltage of the panels to the voltage of the battery, such as DC/DC converters.

3.2 Solar cells and DC/DC converters

Boost DC/DC converters are switch based controllers that are able to step up their output voltage higher than their input voltage. When connected to a solar panel as input, a DC/DC controller is able to adjust the panel's operating point.
A basic converter theory is described below.

3.2.1 Boost converter theory

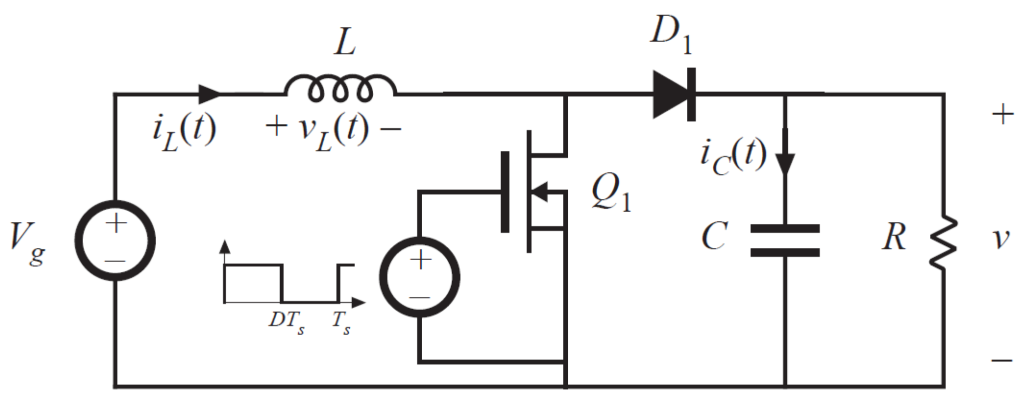

Figure 3.6: Model of a BOOST converter

A DC/DC boost converter consists of an inductor L, a switch Q_1, a diode D_1, a capacitor C and an input voltage V_g. The controller's topology is shown in Figure 3.6 from [11]. The duty cycle, D of the pulse of period T_s sent to the switch turns it either "ON" or "OFF". The magnetic energy stored in the inductor while the switch is "ON" can be used to boost the output voltage when the switch is "OFF". The capacitor enables a steady DC output voltage, V_{out}. The conversion ratio$M(D)$ of the boost converter is as follows:

$$M(D) = \frac{V_{out}}{V_g} = \frac{1}{1-D} \tag{3.5}$$

Assuming a small ripple approximation of the current in the inductor, a fixed input voltage, V_g, combined with a fixed duty cycle, D, ensures a steady output voltage V_{out}.

Considering an efficiency η of the converter, the output power is then:

$$P_{in} = \eta^{-1} P_{out} \tag{3.6}$$

Connecting the output to a load, R induces a current to flow.
The relation between the input and output current can then be found:

$$\begin{aligned}
P_{in} &= \eta^{-1} P_{out} \\
V_{in} I_{in} &= \eta^{-1} V_{out} I_{out} \\
\iff I_{in} &= \eta^{-1} \frac{V_{out}}{V_{in}} I_{out} \\
&= \eta^{-1} \frac{I_{out}}{1-D} \\
I_{in} &= \eta^{-1} \frac{V_{out}}{R(1-D)} \\
I_{in} &= \eta^{-1} \frac{V_{in}}{R(1-D)^2}
\end{aligned}$$

The input current can be determined through the duty cycle and the load of the converter. Considering a perfect converter with η=1, the equivalent resistance R_{in} seen by the input is equal to:

$$R_{in} = R(1-D)^2 \tag{3.7}$$

The equivalent resistance can be adjusted through the duty cycle. As D is always lower than 1, R_{in} can only be lower than R.

Most of the converters control their duty cycle to output a steady output voltage, such as the four DC/DC converters used in the power distribution part of the EPS. These converters are BUCK converters and not BOOST as described here. Their topology is such that the output voltage of the controller is lower than its input voltage.
The equivalent resistance R_{in} and conversation ratio $M(D)$ of the BUCK converter are found similarly:

$$R_{in} = \frac{R}{D^2} \tag{3.8}$$

$$M(D) = \frac{V_{out}}{V_g} = D \tag{3.9}$$

Connecting the solar panels directly onto them would lead to an unstable solar panel's operating point.
As the power consumption of the satellite slightly increases, more current is drawn from the panel, moving its operating point to the left of its I-V curve. The panel's voltage, V_g, decreases accordingly. From equation 3.8, as the controller adjusts the duty cycle to keep its output voltage constant, the duty cycle increases. The equivalent resistance R_{in} seen by the panel decreases.
From Figure 3.4, it is known that reducing the load connected to a solar panel moves its

operating point to the left of its I-V curve, reducing its voltage.
Hence, the operating point of the panel would not cease to move to the left of its I-V curve , until no more power can be harvested.

Another type of controller, based on the equivalent resistance R_{in} is needed to adjust the load seen by the solar panel and maintain its operating point as close as possible to the MPP. This type of controller is known as MPPT controller.
The output voltage of the converter is however not steady anymore.
Different MPPT control algorithms able to operate a cell at its MPP are discussed in chapter 4.

3.3 Conclusion

In this chapter, the constraints imposed by the solar panels and the nominal voltage of the 2sp1 battery pack on the design of the EPS are introduced.
It is shown that the solar panels cannot be directly connected to the four DC/DC buck converters of the power distribution part of the EPS. It is also shown that two solar panels cannot be connected in series.
However, as the voltage of the panels must be boosted to supply both the buck converters and to charge the battery, a MPPT boost controller is required to manage the solar panels' I-V curve.

4 Analysis of the MPPT strategy

The aim of the MPPT algorithm is to adjust the duty cycle of the converter in order to move the operating point of the solar cell towards its MPP.
Below, three main algorithms commonly used in low power application are summarised and discussed:

1. Constant Voltage
2. Perturb & Observe
3. Incremental Conductance

The goal of this section is to find out which algorithm suits our application best. Their advantages, drawbacks, complexity and flight heritage are factors contributing to the final decision.

4.1 Constant Voltage

The constant Voltage (CV) method is the simplest method since it consists in only sampling the voltage of the solar cell and adjusting the duty cycle of the converter through a Proportional-Integral (PI) controller.

This algorithm is based on the assumption that the voltage of maximum power, V_{MPP}, compared to the open-circuit voltage, V_{OC}, is a nearly constant ratio, K[12]:

$$\frac{V_{MPP}}{V_{OC}} = K(<1) \tag{4.1}$$

This K ratio is fixed in the script of the controller. According to a study of the Brunel University of London, the ratio K is often found to be between 70% and 80%[13].
The K factor for OUFTI-2 solar panels in different insolation and temperature conditions can be measured from the simulation made in chapter 3. Under different insolations at 28 °C, the K factor varies between 81.3 and 84.8%.
When the temperature varies, although the maximum power voltage varies significantly, so does the open circuit voltage. The K ratio is then also quite stable and ranges from 81.3 to 83.9%. Hence, the assumption is verified in our application.

The controller disconnects the cell from the load periodically to measure the cell's open-circuit voltage. The maximum power voltage is then computed through the K ratio. The duty cycle of the converter can then be adjusted to move the operation point of the cell towards its MPP.

4.2 Perturb and Observe

A second method to track the maximum power of a solar panel is the perturb and observe (P&O) algorithm, the most commonly used algorithm. The principle is to perturb the operation point of the cell by changing its voltage or current, and checking the variation of power. The duty cycle is adjusted accordingly to increase the input power.
Figure 4.1 from an article of the Marmara University in Istanbul[14] shows the flow chart of the algorithm.

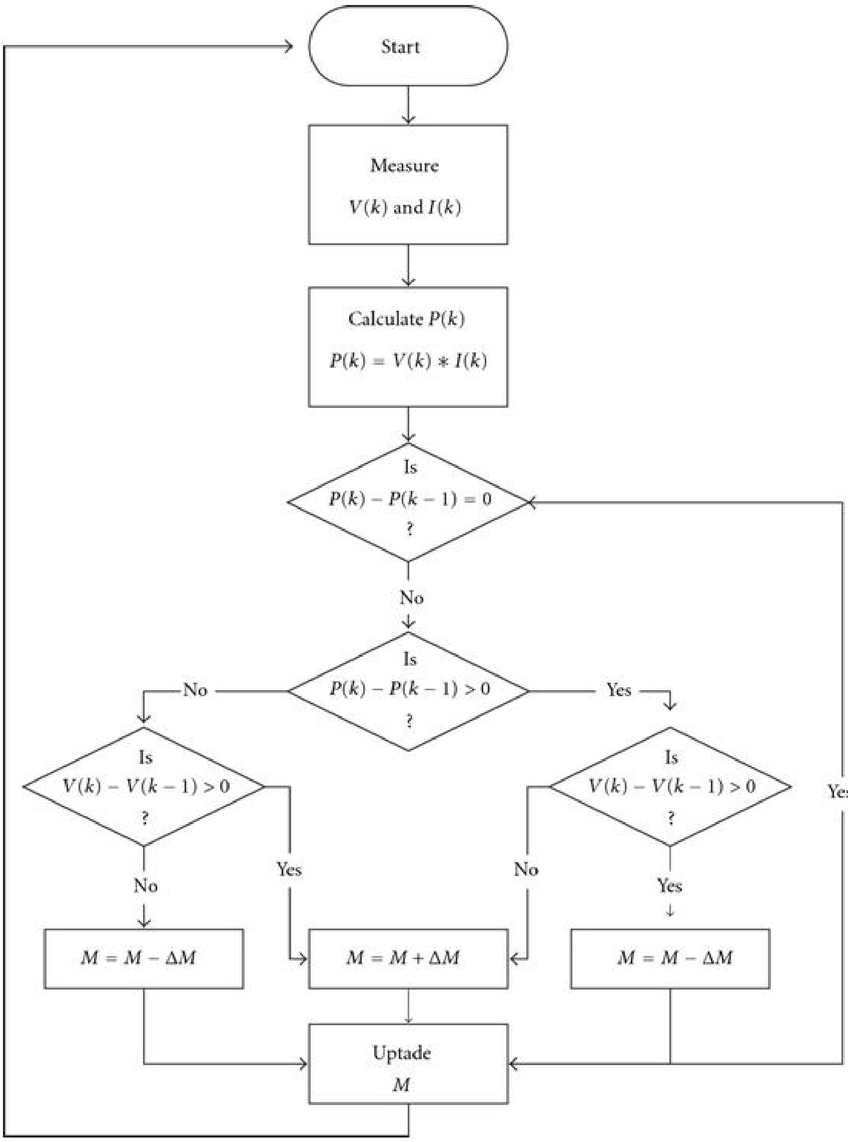

Figure 4.1: Flow chart of the perturb & observe algorithm

The voltage and current of the cell are sampled and their product, $P(k)$ is computed.
The values are stored in memory and the duty cycle, called M in this chart, is then slightly changed. Both voltage and current are sampled again and compared to the previous power sample.
A duty cycle near 1 (short circuit of the solar panel) corresponds to left side of the P-V curve of the solar panel, as can be seen in Figure 3.3 from the previous chapter. The right side of the P-V curve corresponds to a low duty cycle.

Comparing the variation of voltage, $\Delta V = V(k) - V(k-1)$, and power, $\Delta P = P(k) - P(k-1)$P, leads to four possible scenarios.
According to the shape of the power curve, if both ΔV and ΔP are positive (inv. negative), then the operating point is located on the left of the MPP. The duty cycle must then be decreased (inv. increased) to move towards the MPP. If ΔV and ΔP have different signs, the operation point is currently at the right of the MPP. If ΔV is positive then the duty cycle must be increased.
Then, the duty cycle is updated and new samples are stored.

The simplicity and the ability to track the real MPP no matter the state of the solar panel is the reason of its wild utilisation.
However, as the resolution of the duty cycle is finite, oscillations occur around the MPP at each cycle of the algorithm.
Furthermore, if the insolation on the solar cell changes faster than a time step of the algorithm, the MPP of the cell can change without the controller noticing it.

4.3 Incremental Conductance

A third method, the Incremental Conductance (IC), was designed by students from Sega University in order to deal with the drawbacks of the P&O algorithm
This method can determine when it operates at the MPP and then stops the perturbations. When the MPP changes, the direction in which the operation point must be perturbed is known. The direction is deduced from the relationship between the incremental conductance of the solar panel and its instantaneous conductance [12].
To understand the principle of this algorithm, one must express the derivative of the P-V curve of the cell:

$$\begin{aligned} \frac{dP}{dV} &= \frac{d(IV)}{dV} \\ &= I + V\frac{dI}{dV} \end{aligned}$$

The maximum power point is then found at the root of this function:

$$
\begin{aligned}
I+V\frac{dI}{dV}&=0\\
V\frac{dI}{dV}&=-I\\
\frac{dI}{dV}&=-\frac{I}{V}
\end{aligned}
\tag{4.2}
$$

Equation 4.2 links the incremental conductance of the solar panel on the left hand side with the opposite of its instantaneous conductance on the right hand side. At the MPP, this two values should be equal.
Comparing the two terms allows to notice a change in the I-V curve and spot in which direction the MPP has moved.

In this algorithm, the current voltage $V(k)$ and current $I(k)$ of the solar panel are sampled, stored and subtracted to the previous samples, giving ΔV and ΔI. The incremental conductance can then be computed. By comparing it to the instantaneous conductance, $\frac{I(k)}{V(k)}$, it can be known whether to increase or decrease the voltage of the solar panel.
The cycle is repeated until both ΔV and ΔI are null, then the MPP has been found.

This method has the advantage to not oscillate around the MPP. Furthermore, the algorithm can detect in which direction the instantaneous MPP is located compared to the actual operation point, allowing the MPP to be tracked even under rapidly changing insolation.

However, the drawback of this method is its complexity and the higher computation power requested through the division comparisons compared to the P&O algorithm.

4.4 Comparison of the different methods

After reviewing the 3 methods, the simplest methods are found to be the CV and P&O algorithms, demanding only basic chips for the sensing and computations operations.
Low complexity algorithms often consumes less power, a significant advantage when it comes to low power CubeSat.
Simpler design also decreases the amount of space used on the PCB and increases the reliability of the project.
For a same level of complexity, the P&O algorithm has the advantage to track the real MPP of the solar panel, while the CV method only tracks what it think to be the MPP. Hence, the P&O algorithm is preferred.
To conclude from Table 4.1, the P&O algorithm combines a low complexity and does not disconnect the solar panels from the load. If the controller's frequency is high enough to react

	Constant Voltage	Perturb and Observe	Incremental Conductance
Complexity	Low	Low	Medium
Measured Parameters	Voltage	Current & Voltage	Current & Voltage
Periodic disconnection of the solar panel	Yes	No	No

Table 4.1: Comparison table of the Constant Voltage, the Perturb & Observe, and the Incremental Inductance MPPT algorithms

to the change of insolation due to the spin of the satellite, the P&O algorithm is a safer option than the more complex IC method.

The SPV1040 from `Texas Instrument` [15], implements this P&O algorithm and suits the requirements of our application.

4.5 Non exhaustive review of MPPT use in CubeSat applications

Flight heritage is an important characteristic to check when designing a spacecraft system. Several missions with equivalent or close solar and battery configurations were analysed in order to gather some practical examples [16][17][18][19][20].
This section introduces their main information as well as their batteries and solar panels topology and management systems.

1. Kufasat from the Technical Institute of Kufa, Iraq:
    - Launch: Planned for 2020
    - Payload: Imaging purpose
    - Solar panel output voltage at maximum power point: 4.2V
    - Battery nominal voltage: 4.2V
    - MPPT algorithm: P&O algorithm through the SPV1040 Boost solar charger
2. AALTO2 from Aalto University, Finland:
    - Launch: April 18, 2017
    - Payload: Unspecified
    - Solar panel output voltage at maximum power point: 4.2V
    - Battery nominal voltage: 4.7V
    - MPPT algorithm: P&O algorithm through the SPV1040 Boost solar charger

3. KySat from Kentucky Space, USA:
    - Launch: March 4, 2011
    - Payload: Unspecified
    - Solar panel output voltage at maximum power point: 4.2V
    - Battery nominal voltage: 7.4V
    - MPPT algorithm: Homemade P&O algorithm and boost solar charger
4. AAU from Aalborg University, Denmark:
    - Launch: June 30,2003
    - Payload: CMOS digital camera
    - Solar panel output voltage at maximum power point: 4.2V
    - Battery nominal voltage: 7.4V
    - MPPT algorithm: Homemade P&O algorithm and boost solar charger
5. NUTS from the Norwegian University of Science and Technology, Norway:
    - Not launched yet
    - Payload: Infrared camera for Earth's observation
    - Solar panel output voltage at maximum power point: 2.2V
    - Battery nominal voltage: 7.4V
    - MPPT algorithm: Two SPV1040 Boost solar charger in series

4.6 Conclusion

None of the satellites of the review, except AAU, meet the same requirements and topology as OUFTI-2, which are: a solar panel output voltage at maximum power point of 4.5V; a 7.4V battery nominal voltage.
AAU implements a homemade MPPT controller. This solution is not considered here yet. A first simpler approach with already existing component is preferred to increase the reliability of the design.
For the other CubeSats, it can be seen that the SPV1040 is wildly use to control the I-V curve of a solar panel to a single LiPo battery cell. The chip can also be used in series to boost a 2s1p LiPo battery pack, such a configuration is used in the NUTS CubeSat.
The SPV1040 chips presents a flight heritage and suitable characteristics for our application and deserves further investigation.

5 SPV1040 and OUFTI-2

The SPV1040 device is a MPPT boost controller implementing a P&O algorithm with a 100kHz fixed frequency. The controller monitors its output voltage in order not to exceed a voltage threshold V_{lim} that can be programmed.

The oscillations of the solar cell's voltage around its MPP, intrinsic to the P&O algorithm, were measured by a thesis from the university of OSLO about their cubeSat cubeSTAR [21]. The measurement was carried out with the same solar cell as OUFTI-2, a spectrolab UTJ solar cell under an insolation of 100W/cm^2 and at 28 °C.
The period of the oscillation is found to be 15 ms.[21].
A first comparison of the changing insolation conditions is made to ensure that the chip is able to track the MPP of the solar cells.
This first approach is simplistic but allows to get an order of magnitude of the maximum spinning rates supported by the chip.
The first assumption is that the MPP of a solar panel is considered to have changed when the panel has turned 10°away from the sun, i.e. 0.17rad. Based on the 15ms oscillations, the maximum spinning rotation of the satellite is $\frac{0.17}{0.015} \simeq 11.7$ rad/s in any direction.
From section 2.3.2, it is known that the passive attitude control of OUFTI-2 stabilises the rotation of the CubeSat.
Furthermore, from the thesis of Vincent-François Lavet about the attitude control of OUFTI-2 [6], a high initial spin hypothesis would be of the order of π rad/s.
Hence, the high control frequency of the SPV1040 enables the chip to track the MPP of the solar panels even in the worst case spinning conditions undergone by OUFTI-2.

5.1 Principle

The SPV1040 has for aim to transfer a maximum amount of power from the solar cells to the load. However, it has some limitations.
The first one is that it cannot transfer more power than the solar cell's MPP it is controlling.
The second limitation comes from its output voltage threshold.

As the rest of the satellite is not implemented yet, the power consumption is simulated by a load, R. Based on the value of the load connected to the controller, three regimes of the SPV1040 can be observed.
Figure 5.1 is a representation of the different behaviours of the SPV1040. The loads are plotted onto the I-V curve of one of OUFTI-2's solar panel at G=1 and 28 °C.
The maximum power of a panel in these conditions is 1948 mW.

The scripts implemented in chapter 3 were used to plot the figure.

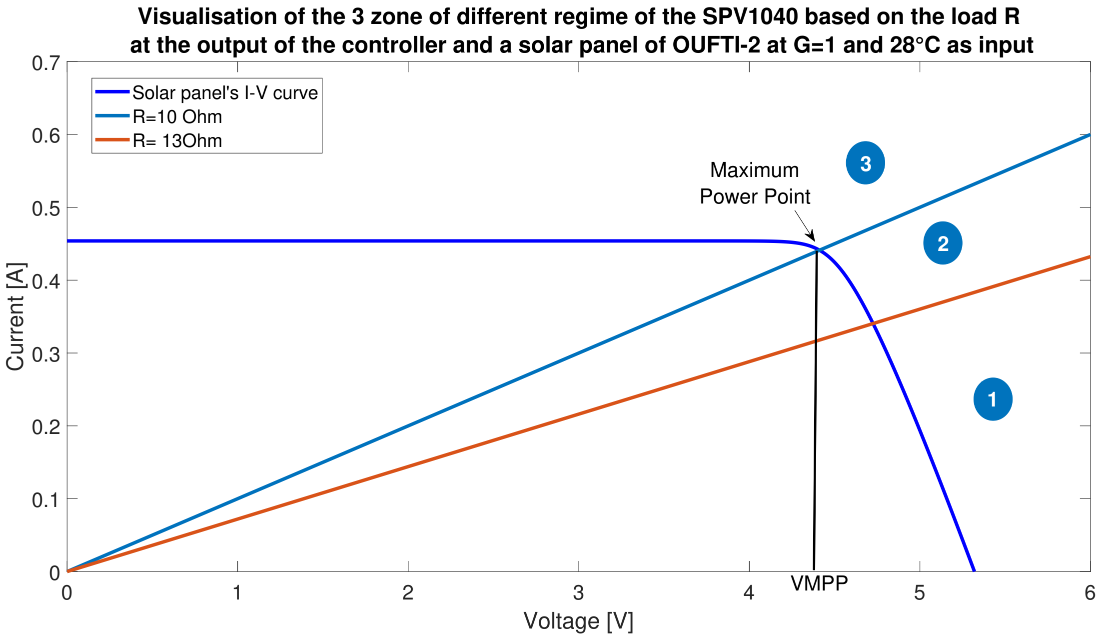

Figure 5.1: Visualisation of the 3 regimes of the SPV1040 based on the load R at the output of the controller and a solar panel of OUFTI-2 at G=1 and 28°C at its input

Let's start the reasoning with an infinite load R, which correspond to an open-circuit scenario. The operating point of the panel is located at the open-circuit voltage V_{OC} and no current is drawn.
If the cell is illuminated enough V_{OC} is higher than 0.3V, the minimum voltage for the SPV1040 to activate.
The duty cycle, D, of the converter is null at the beginning, i.e. the solar cell is always connected to the load R. Hence the equivalent resistance seen by the panel, R_{in}, is equal to the load, R, which fixes the operating point of the solar cell to the intersection of their I-V curves.
The P&0 algorithm then starts and the duty cycle of the converter is increased.
As R_{in}=$R(1-D)^2$, the equivalent resistance, R_{in}, decreases and the operating point of the solar panel is moved toward its MPP.
The change of current in the inductor of the controller boosts the voltage of its output compared to its input.
As the SPV1040 blocks its output voltage to the threshold voltage, V_{lim}, the maximum power consumed, P_{cons}, by a load, R, is limited:

$$P_{cons}= \frac{V_{lim}^2}{R}$$

The first regime of the SPV1040 occurs for high resistance loads such that:

$$R > \frac{V_{lim}^2}{P_{MP}}$$

where P_{MP} is the maximum power of the solar panel.
For a solar panel of OUFTI-2, under a mean solar constant of 136.7mW/cm^2, at 28°C, and if the threshold voltage of the SPV1040 is set to 5.2V, the minimum load R for this operation mode is $R = \frac{5.2^2}{1.948} \simeq 13\Omega$.

In this regime, the SPV1040 has an output voltage equal to its threshold. The power harvested is limited by $\frac{V_{lim}^2}{R}$.
When the power consumption increases, i.e. when the load decreases, a second operation regime is reached.

In this regime, the equivalent load, R_{in} is such that the MPP of the solar panel is achieved before the output threshold voltage of the controller. This output voltage is then:

$$V_{out} = \frac{V_{in}}{1-D} < V_{lim}$$

This regime is for loads such that:

$$R \in [\frac{V_{MPP}^2}{P_{MP}}; \frac{V_{lim}^2}{P_{MP}}]$$

where V_{MPP} it the voltage of the panel operating at the MPP.
In the same conditions as before, the boundary loads correspond to $R \in [10-13]\Omega$.

When the load is such that:

$$R > \frac{V_{MPP}^2}{P_{MP}}$$

the panel's operating point is located before the V_{MPP}. Although the goal of DC/DC converter is to adjust the load of the solar panel, as the SPV1040 is a boost controller, it can only adjust the load to lower resistances, as explained in section 3.2.
In this mode, the maximum power extracted from the panel is achieved for a duty cycle null, but is always lower than the panel's MPP. Hence the input voltage is equal to the output voltage, which is function of the operating point of the load.

The chip was tested with a solar panel of OUFTI-2 in a cloudless day and a variable resistor, using a homemade PCB, described in chapter 9.
The voltage threshold of the chip for the test was programmed to 5.2V.
The efficiency of the chip and the harvested power were measured for one resistance of each operating regime.

Table 5.1 summarises the theoretical and measured power and output voltage of the SPV1040 for each regime.

SPV1040	Parameters	Regime 1 $R > \frac{V_{lim}^2}{P_{MP}}$	Regime 2 $R \in [\frac{V_{MPP}^2}{P_{MP}}; \frac{V_{lim}^2}{P_{MP}}]$	Regime 3 $R > \frac{V_{MPP}^2}{P_{MP}}$
Theoretical Summary	Power harvested P_{in}	$\frac{V_{lim}^2}{R}$	P_{MP}	$\frac{V_{in}^2}{R}$
	Output voltage V_{out}	V_{lim}	$[V_{MPP} - V_{lim}]$	[0-V_{MPP}]
Practical measurements	Input power, P_{in} [mW]	578.4	1131.6	974
	Output voltage V_{out} [V]	5.2	5.12	3
	Load resistance R [Ω]	50	25	10
	Efficiency η [%]	93.5	92.6	92.4

Table 5.1: Summary of the power consumed and the output voltage of the SPV1040 for the 3 operation regimes

It can be seen that the maximum power of the solar panel achieved, 1131.6 mW, is lower than the 1948 mW expected and the load values for each regime are higher than the one expected by the simulation in Figure 5.1.
This is due to the fact that the sun's energy received on Earth is lower than the one receives above the atmosphere.
Hence the panel's I-V curve on Earth is lower than the one simulated and the boundary resistances of each regime are higher.

A part from these remarks, the 3 separate regimes were observed and the output power and voltage match the predictions.
Furthermore, the efficiency of the SPV1040 is measured between 92.4% and 93.6%.

In a the final EPS design, the power consumption is fixed and does not depend on a load. As the SPV1040 cannot longer act on the output voltage to regulate the power consumed by the load, only two operations regimes can be observed.

The first regime is for power consumptions lower than the maximum power of the solar panels. In this mode, the power harvested is equal to the power consumed and the output voltage is fixed at the threshold voltage.
The second regime is for higher power consumptions. In this case the voltage of the solar panel

drops and no more power is transferred.

For OUFTI-2, the power consumption can vary based on the operations of the satellite and is not always equal to the maximum power produced by the solar panels. To operate the solar panels as close to their MPP as possible, the batteries have then a role of buffer: increasing the power consumption when charging, and the opposite when discharging.
When the batteries are full, the power harvested is then limited to the power consumed. Otherwise, the charge of the battery is used to get the maximum out of the solar panels.

5.2 Series configuration

The limit output voltage of the SPV1040 controller is fixed to 5.5V [15]. As this voltage is not enough to charge a 2s1p LiPo battery, a series configuration of two SPV1040 is considered. Such a configuration is described in the datasheet of the SPV1040, provided by the manufacturer [15][22].
Figure 5.2 represents the test circuit of the configuration.

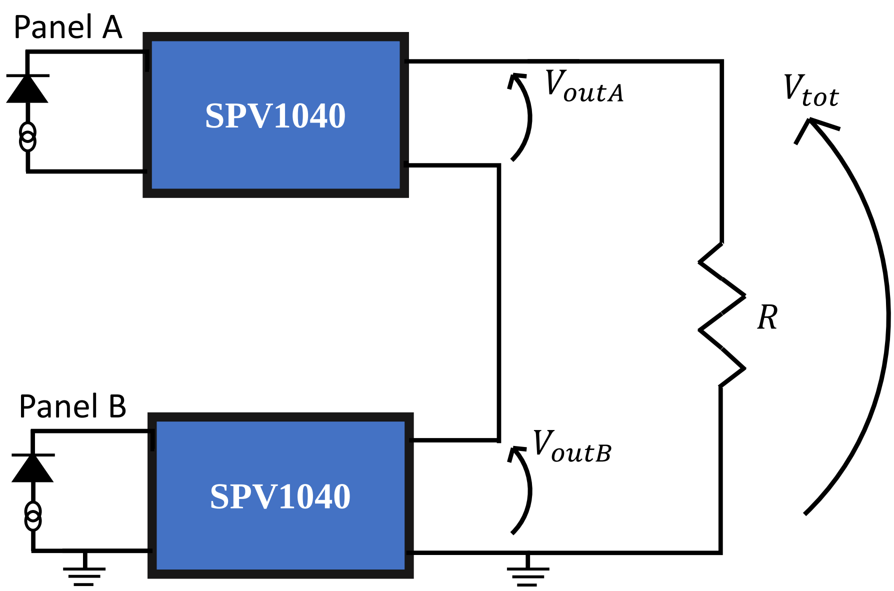

Figure 5.2: Test circuit of two SPV1040 MPPT controllers in series

The topology imposes the same output current, I_{out}, for both chips.
Based on their I-V curve, the two panels have different MPP. Let's assume that panel A is less illuminated than panel B. Hence, the maximum power of panel A, P_{MP_A} is lower than the one of panel B, P_{MP_B}.

When the same voltage threshold, V_{lim}, is set for both SPV1040, each chip contributes in its own way to the total power harvested. The power contribution of each SPV1040 is function of its output voltage, V_{outA} and V_{outB}.

The same analysis as for a single SPV1040 is carried out.
As the output load decreases, the total output voltage, V_{tot} and the power consumed by the load varies.
Three main operating regimes are observed, which corresponds to combinations of the operating regimes of singular SPV1040.
In order to clarify the understanding of each regime, a power analysis based on the power consumption of the load and the maximum power point of each solar panel is carried out.
Table 5.2 summaries the theoretical input power and output voltage of the different regimes.
The tests of this configuration are performed in chapter 7.

SPV1040	Parameters	$P_{cons}<P_{MP_A}+P_{MP_B}$		$P_{cons}>P_{MP_A}+P_{MP_B}$
		Regime 1 $\frac{P_{cons}}{2}<P_{MP_A}$ $\frac{P_{cons}}{2}<P_{MP_B}$	Regime 2 $\frac{P_{cons}}{2}<P_{MP_B}$ $\frac{P_{cons}}{2}>P_{MP_A}$	Regime 3
Panel A	Power harvested P_{outA}	$\frac{P_{cons}}{2}$	P_{MP_A}	0mW
	Output voltage V_{outA}	V_{lim}	$\frac{P_{MP_A}}{I_{out}}$	0V
Panel B	Power harvested P_{outB}	$\frac{P_{cons}}{2}$	$P_{cons}-P_{MP_A}$	0mW
	Output voltage V_{outB}	V_{lim}	V_{lim}	0V
Total Output	Output voltage V_{tot}	$2V_{lim}$	$\frac{P_{MP_A}}{I_{out}}+V_{lim}$	0V

Table 5.2: Summary of the three operation regimes of two SPV1040 in series based on their power consumption

The first distinction of behaviour corresponds to power consumptions such that:

$$P_{cons}<P_{MP_A}+P_{MP_B}$$

In this way, 2 regimes are observed.
Either $\frac{P_{cons}}{2}$ is lower than the maximum power of both solar panels. Then both output voltage panel is limited by the voltage threshold of the SPV1040, V_{lim}, and each panel contributes to half of the power consumed.
Either $\frac{P_{cons}}{2}$ is lower than the maximum power of one panel, panel A in this case. Then the SPV1040 of this panel is giving the maximum power. As the output current, I_{out}, is the same

for both chips, the output voltage of panel A is simply:

$$V_{outA} = \frac{P_{MP_A}}{I_{out}}$$

The second panels must then provide the rest of power.
The total output voltage is then fixed by:

$$\begin{aligned} V_{tot} &= \frac{P_{MP_A}}{I_{out}} + V_{lim} \\ &\in [V_{MPP_A} + V_{MPP_B}; 2V_{lim}] \end{aligned}$$

where V_{MPP_A} and V_{MPP_A} are respectively the voltage at maximum power of panel A and B. As seen in chapter 3, about the solar panels of OUFTI-2, the voltage of the MPP slightly changes based on the insolation and temperature. The lowest V_{MPP} that can be reached for one of OUFTI-2's panel is 3.62V. Hence the output voltage of the bus will always be higher than 7.24V.

When the power consumption is higher than the sum of maximum power of both panels, then the controllers are not able to supply the load and the voltage of both chips drops until no more power is transferred.
Hence, the SPV1040 ensures to get the most power out of the solar panel, but is limited by the consumption of the satellite and cannot produce more than what is consumed by the satellite.

It must be ensured that the solar panels can always provide more than the power consumption of the satellite.
This is ensured in chapter 7.

5.3 SPV1040 & Semi-regulated bus

This topology of SPV1040 in series is also used in the EPS of the NUTS CubeSat, and no battery charger must be used, as can be seen in Figure 5.3 [20].
In this topology, the batteries are directly connected onto the output of the SPV1040 controllers in series. The total output voltage of the controller is then fixed by the voltage of the batteries, V_{bat}.

The Norwegian satellite uses each MPPT controller on a single solar cell. NUTS is a 2U cubesat equipped with 18 solar cells. Four on each side and two on the top side.
A depiction of the configuration of one lateral side of the satellite, i.e. 4 solar cells, can be seen in Figure 5.3.
The Maximum power voltage of one cell, V_{MP}, is then only 2.2V. MPPT controllers of solar cells from the same side are connected in series of 2. Then all pairs of controllers are connected

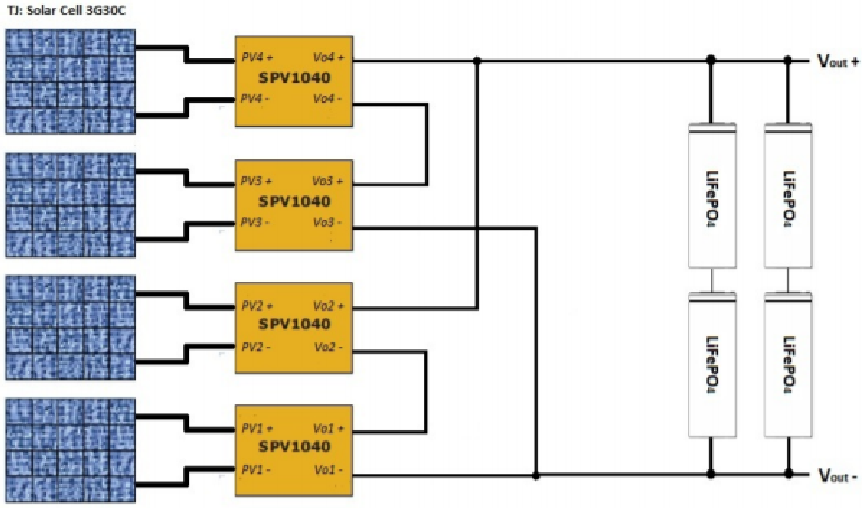

Figure 5.3: Solar cells connection in the NUTS CubeSat

in parallel to the battery and the rest of the satellite through an unregulated bus.

Assuming that cells on the same side have the same I-V curve and that the battery cells are balanced, the SPV1040 are used to directly charge the batteries. In this case, the input power of each of the two SPV1040 connected in series, is the same. The output voltage of each controller is then also half of the total output voltage V_{bat}.
The threshold voltage of each chip is set to 3.6V for each of them, half of the maximum battery voltage. This ensures the SPV1040 to stop the charge when the batteries are charged.

However, our topology is different.
The input of the MPPT controller consists in two solar cells in series whose V_{MP} can range from 3.62V to 5V depending on the temperature and the insolation of the panel. The maximum voltage of the battery is 8.4V, thus the threshold voltage of each controller should be set to 4.2V to stop the charge when the batteries are full.
However, as the SPV1040 is a boost controller, it is activated only when its input voltage is lower than its output voltage. Setting the output threshold to 4.2V would only activate the MPPT controller when the panels operate under 4.2V. Therefore, the panels could not always operate at MPP.

In order to get over this problem, a semi-regulated bus, or sunlight bus, connecting the MPPT controllers to the four DC/DC converters is considered. The batteries are then decoupled from the bus via a battery charger (BCR).

Figure 5.4 is a representation of the semi-regulated bus considered for OUFTI-2.

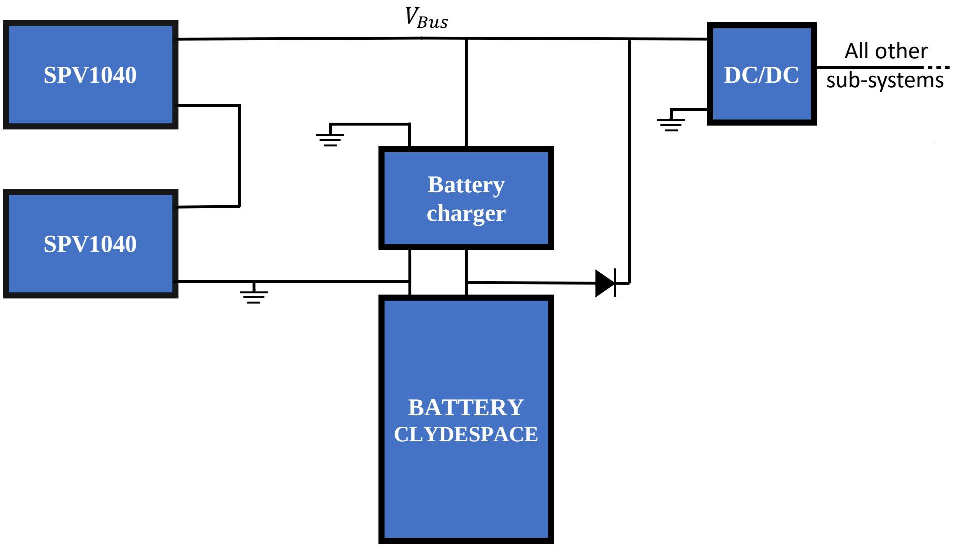

Figure 5.4: Illustration of a sunlight bus

The solar panels controllers in series with a threshold voltage higher than 4.2V directly supply the satellite and ensure a maximum power input. A battery charger enables a safe charge of the battery from the bus voltage, which is twice the threshold voltages of the SPV1040. When the MPPT controllers are not able to power the satellite, due to eclipse or high consumption operation of the satellite, then the batteries can discharge into the bus to supply the satellite and the voltage bus is now fixed by the voltage battery V_{bat}.
A diode prevents the battery from being charged directly from the MPPT controllers.

The choice of a BCR is discussed in the next section.

6 Analysis of the Battery management strategy

The semi-regulated bus design considered due to the requirements of the solar panels and the battery implies a battery charger (BCR).
This chapter has for goal to review the charging methods and protection features of a Lithium Polymer (LiPo) battery cell in order to know which one to use for our application.

6.1 Lithium-Polymer battery

6.1.1 Theoretical approach

LiPo battery cells are high energetic densities solutions compared to other traditional battery cells such as Lithium-Ion.
However, left unregulated, a LiPo can lead to dangerous hazards. The cell must be kept in a specific temperature range. Under/over voltage and overcurrent protection features must be ensured in order to prevent the ignition of the cell.

A proper charging method as well as a small Depth of Discharge (DoD) of the battery is the key to increase the lifespan of the battery. The recommended DoD by the manufacturer is 20% [8]. Figure 6.1 from the datasheet of the battery manufacturer [8] is a table of the voltages of one battery cell measured at different DoD at two different discharge rate.

As the battery is made of two balanced cells in series, the battery voltage for a certain DoD is simply twice the value of one cell's voltage.
The recommended discharge current, C, is 1.3A. Figure 6.1 compares then the voltage of the battery cell at several DoD step for two discharge currents of 260 mA and 26 mA.
From the power budget, the consumption of the satellite is 1231mW with no transmission and 5971mW when a transmission is operated. In order to estimate the respective discharge currents of each consumption, a mean voltage battery of 8.2V is assumed. the discharge currents are found to be 153mA and 728mA, i.e. C/8.5 and C/2.
The lowest battery voltage for a same level of discharge occurs for the highest discharge current. A linear approximation allows to estimate the battery voltage of a cell discharge with a current of 728mA. At a DoD 20% the voltage of the cell is minimum 3.9V in our application.
The voltage of our battery pack, two battery cells in series, is thus expected to range between 7.8V and 8.4V.

DoD (%)	Voltage of cell discharged at C/5 (V)	Voltage of cell discharged at C/50 (V)
0	4.2	4.2
5	4.08	4.14
10	4.03	4.07
15	3.98	4.03
20	3.93	3.98
25	3.9	3.95
30	3.86	3.92
35	3.82	3.98
40	3.79	3.95
45	3.77	3.82
50	3.75	3.8

Figure 6.1: Voltage of a Clydespace battery cell as a function of its depth ofdischarge

6.1.2 Constant current - constant voltage charging method

In order to charge a LiPo battery cell, a constant current - constant voltage (CCCV) method must be applied.
In the first stage of the charge, a constant current is applied while the tension of the cell increases. When the cell reaches its maximum voltage, the charge mode is changed to a constant voltage mode, as can be seen in Figure 6.2 [23].

The `clydespace` battery offers voltage and current protection but does not regulate the charge. An external BCR implementing the CCCV method is therefore needed in our application. Such method can be implemented either linearly, or with a switch-mode method.
Both methods are summarised below.

6.2 Linear vs Switch-Mode

For a linear CCCV charging method, a simple pass transistor connects the input voltage to the battery voltage and analog comparators allow the monitoring of the charge. A constant

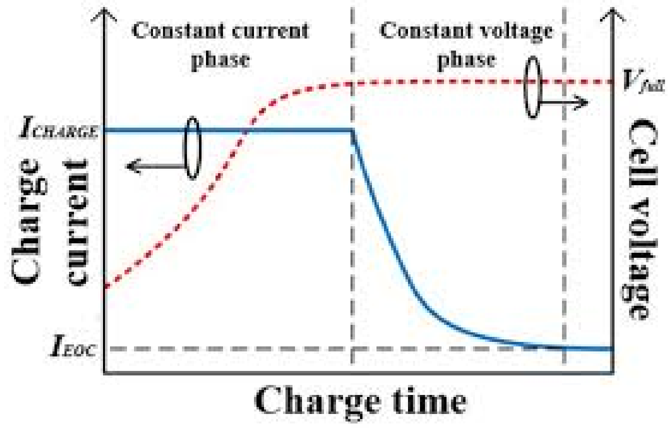

Figure 6.2: Constant current/constant voltage charging method representation

current can be programmed via an external resistor. The voltage of the battery is continuously checked with the maximum battery voltage. When the battery voltage reaches the threshold, the current is reduced until the charge stops.
Several internal comparators allow to stop the charge in certain conditions, e.g. the current, input voltage or temperature thresholds are reached.
Although this method is extremely reliable, the drawback of this method is its power dissipation. The power loss across the pass transistor is found through:

$$P_{loss}=(V_{in}-V_{bat})I_{charge}$$

where V_{in} is the input voltage of the BCR, V_{bat} is the battery voltage and I_{charge} is the charging current.

Switch-mode charger is made of a DC/DC controllers. High power efficiencies up to 99% can then be achieved. In this type of controller, the duty cycle of the converter is function of the charging current feeding the battery.
Digital protections can then be added to monitor the charge of the battery cells.
A significant advantage over the linear charging method is the low power dissipation even if the input voltage is not close to the battery voltage.
However, this controller is bulkier and more complex, decreasing its reliability. Furthermore, the hashing of the current and voltage induces more electromagnetic perturbations for the rest of the satellite.

Two BCR have been identified: The MCP73213 linear dual cells BCR from `Microchip` and the LTC4110 fly-back converter BCR from `Linear Technology`. The linear solution allows a safe and simple implementation but needs an input voltage higher than the battery voltage. Hence this BCR can be used with SPV1040 controllers in series configuration. However, it must be

used with a bus voltage close to the battery voltage, otherwise the power loss quickly rises.
A switch-mode charger allows a wide input range from 5V. That could enable a single SPV1040 as input configuration. However, the 99% efficiency is balanced with a higher risk induced by its complexity.

Depending on the bus configuration and voltage, either one or the other can be chosen. The MCP732123 is preferred with series connection of the SPV1040 controllers whereas the LTC4110 is the only possible option for a bus parallel configuration of the SPV1040 controllers.
Both configuration are tested in the next chapter 7.

For both chargers, a timer regulator which stops the charge after a certain delay is often implemented. This is an additional protection feature meant to protect an overcharge of the battery. A manual restart must be operated after this protection has been triggered. This kind of protection must absolutely be switched off in space application as the overvoltage protection already prevents the overcharge of the battery. Both the MCP73213 and LTC4110 chips offer options without timer.

The power consumed by the charge of the battery is function of the charging current and the battery voltage. As both chargers use a fixed resistance to set the charging current, it can only be set once before the flight. A current value of 130mA is chosen in chapter 10 in order to ensure the battery to charge even when the other sub-systems are used.
The same charging current is chosen for both BCR to compare them more easily.

7 Test and comparison of several relevant architecture designs

In this section, different architecture designs are analysed and compared.
The designs that are considered already satisfy the requirements introduced in the previous sections:

- The solar panels can be connected in parallel but not in series
- A battery charger ensures a safe charge of the battery while decoupling it from the bus
- The design is compatible with a 2 LiPo cells in series battery pack
- The output of the design is compatible with the input of the four step down converters that supply the rest of the satellite

Figure 7.1 represents the required high level architecture in three stages. The maximum ratings of the DC/DC converters are shown to emphasise that the design architecture must respect this constraint. Furthermore, it is known from chapter 6 that the battery voltage can range from 7.8V to 8.4V for a maximum DoD of 20%.

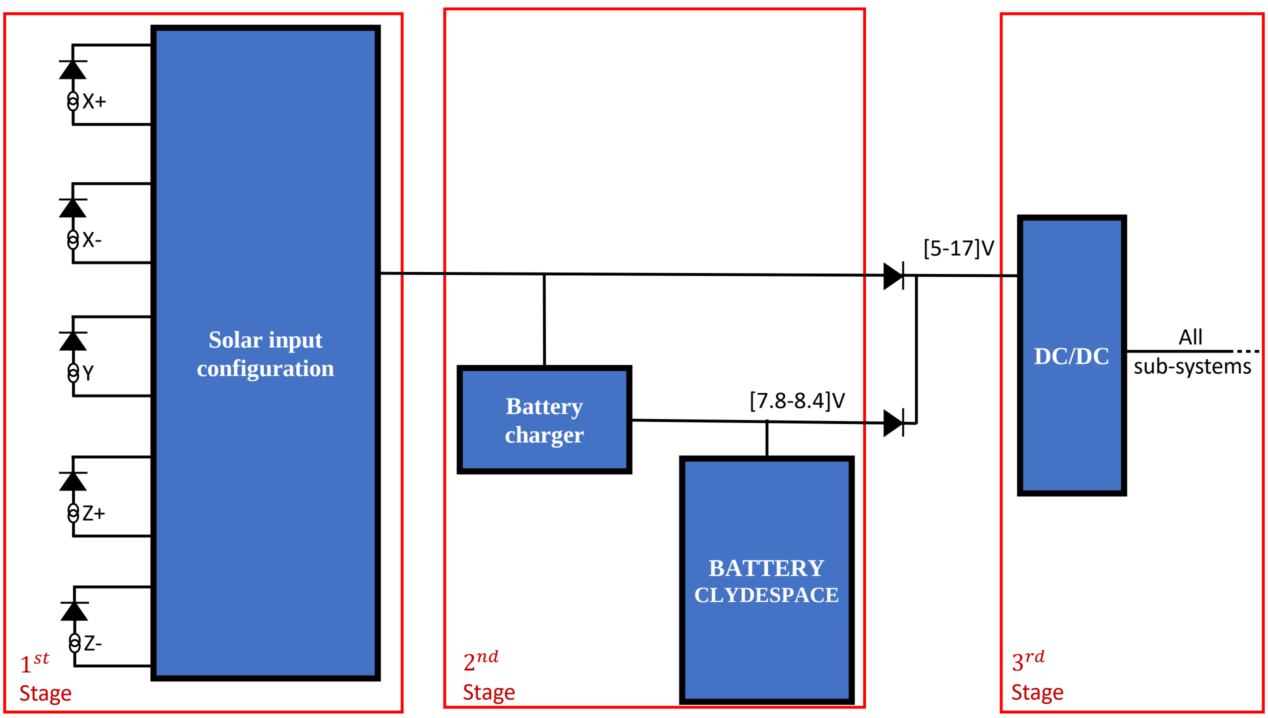

Figure 7.1: Initial requirements for the architecture of the EPS

The 1^{st} stage has for goal to connect all 5 solar panels and to step up their voltage for the other stages.
The five solar panels are identified through their orientation, e.g. X+is the solar panel in the positive X direction. The sixth side of the cubesat is equipped with the antennas.
The load of the panels are then adjusted by MPPT boost controllers.

The output current and voltage of the 1^{st} stage, is function of the configuration of the MPPT controllers. Two configurations of the controllers are discussed here: A series connection of two MPPT controller to reach the battery voltage, or a parallel connection. A parallel connection must then be followed by a boost battery charger, able to charge the battery with a CCCV method and also boost its input voltage to the battery voltage.

The 2^{nd} stage is the BCR and battery block. The BCR can be linear only if the input voltage is higher than the battery voltage, i.e. with a series connection of MPPT controllers. A switching mode BCR can be used as boost battery charger for a parallel configuration of the SPV1040.

Finally, both the output of the 1^{st} and 2^{nd} stages must be compatible with the input of the 3^{rd} stage: four TPS62130 step down converters that supply all other sub-systems of the satellite with steady voltages. The input voltage of the controller, V_{in} has a maximum rating of 17V[24]. As this is a buck controller, its input voltage must be always higher than its output voltage. As the highest steady voltage required by the satellite is 5V, V_{in} must range between 5V and 17V.

Two diodes are in the design in order to ensure that the battery is charged only by the BCR, and that it discharged only when the solar panels cannot provide enough power. This part is discussed in the power path chapter 8.

The differences in the possible designs discussed in this chapter come from the MPPT controllers configuration and the choice of the BCR. The final decision of architecture is based on the comparison of the power efficiency of every stages as well as the reliability of every design.

7.1 Connection of MPPT controllers in series

The first architecture analysed is a connection of two SPV1040 MPPT controllers in series followed by the MCP73213, linear BCR. The first two stages of the architecture, the SPV1040 stage and the linear BCR stage, are tested under different inclination of the panels.
The goal of the test is to ensure that the cascade connection of the MPPT controllers and the BCR is stable. The voltage of the bus is also checked to verify the theoretical results obtained in chapter 5.

From the results of the test, a theoretical comparison of architectures with 2, 3 and 5 MPPT controllers in series is carried out. The decision of which solar panels are connected to each MPPT controller is also discussed for every architecture.

Test of the configuration

Figure 7.2 is a picture of the test set-up. The test took place outside during a cloudless day at 18°C. The solar panels and the 2sp1 battery pack are connected to the homemade development board of the SPV1040 in series and the MCP73213.
This development board is further explained in the chapter 9.

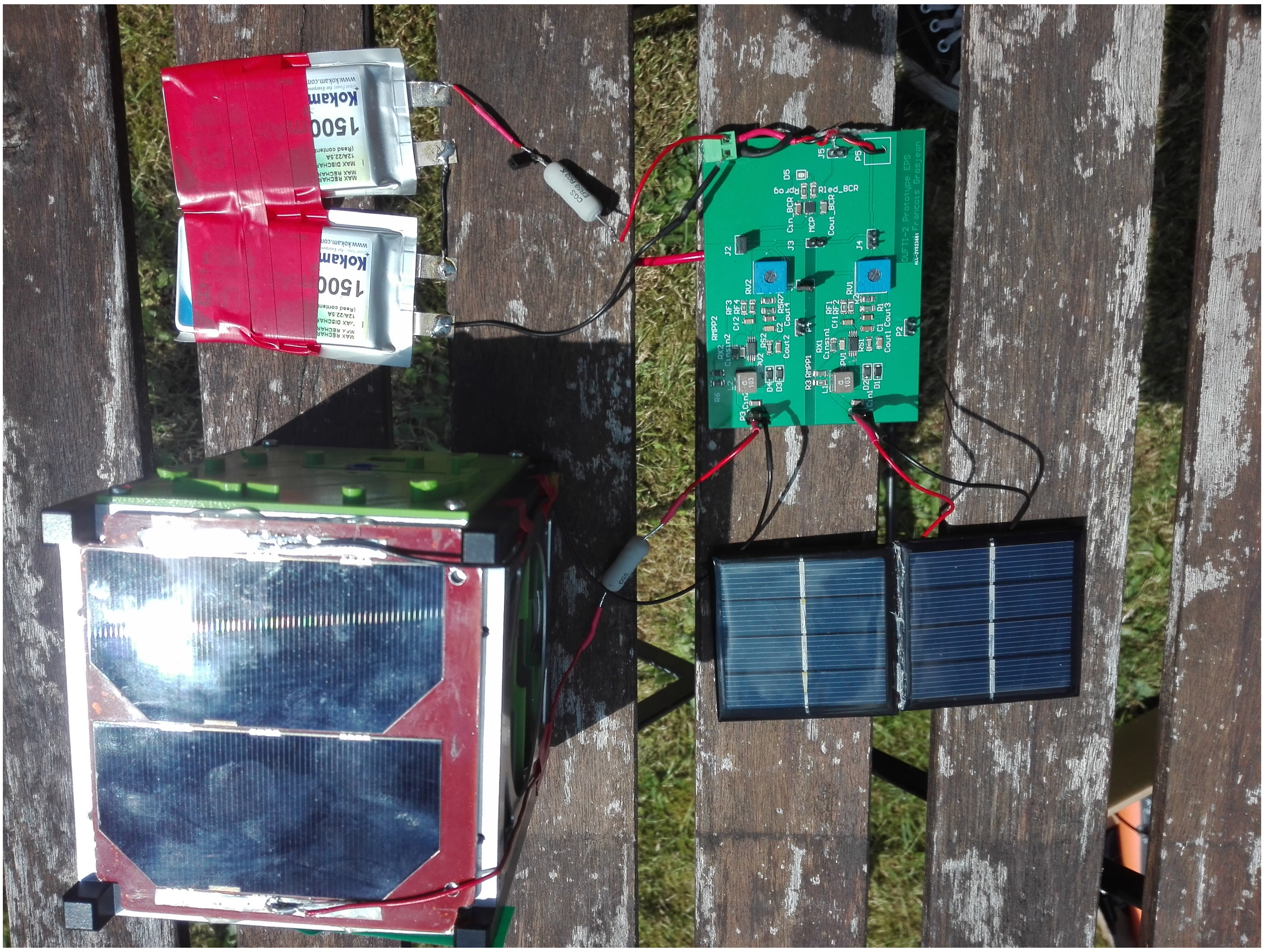

Figure 7.2: Picture of the test set-up of the series configuration

The tests are performed with the following materials:

- Four multimeters TENMA 72-7730A
- Two 30mΩ sense current resistors, 7W, from CGS
- Homemade development board, cfr. chapter 9
- Two 1500mAh LiPo battery cells in series, with a voltage of 8.12V
- One solar panel of OUFTI-2, i.e. two `spectrolab` UTJ solar cells in series
- Two poly-crystalline PV panels in series

As only one solar panel of OUFTI-2 was available, 2 poly-crystalline panels from the development board of the SPV1040 chip were used [25]. A poly-crystalline solar cell can output a maximum power of 200 mW and Table 7.1 presents its electrical characteristics:

Voltage at maximum Power, V_{mp}	1.44V
Current at maximum Power, I_{mp}	135mA
Maximum Power, P_{mp}	194.4mW
Open-circuit voltage, V_{oc}	1.65V
Short-circuit current, I_{sc}	150mA
Efficiency, η	15%

Table 7.1: Electrical characteristics of the Poly-crystalline PV panel under a 1000W/m^2 insolation and at 25°C

Two solar cells connected in series in these lighting and temperature conditions can then output a maximum of 388.8mW at a voltage of 2.88V.
Although these solar cells can generate very low power compared to one OUFTI-2's solar panel, the behaviour of the SPV1040 in series can still be tested.
One must bear in mind that the resulting values are lower than what can be expected in space and with two OUFTI-2's solar panel.

The tests were carried out on cloudless day, i.e. under an insolation power $\simeq$ 1000W/m^2, and at 18°C.
The estimated maximum power of OUFTI2's solar panel can be found through the simulation code made in chapter 3 and is found to be 1438mW at V=4.6V. The theoretical maximum power that both panels can output at full insolation is then 1438+388.8=1826.8mW.

Table 7.2 shows the results of the test when the two MPPT controllers in series are connected to the linear BCR with different inclination of one panel compared to the sun. Panel A is

OUFTI-2's solar panel, and panel 2 is the two poly-crystalline solar cells in series.
The coloured boxes are computed values, whereas white boxes are measured values. The currents and voltages were either measured directly with the multimetre, or via current sense resistors, the equivalent powers are then obtained with the classic formula $P = VI$.

Stages	Parameters	Full irradiation on both panels	Panel A inclined by 45°	Panel B inclined by 90°
Panel A	Input voltage V_{inA}, [V]	4.6	4.65	5.2
	Input current I_{inA}, [mA]	175	170	5
	Input power P_{inA}, [mW]	805	791	26
Panel B	Input voltage V_{inB}, [V]	2.85	2.85	3.2
	Input current I_{inB}, [mA]	135	135	4
	Input power P_{inB}, [mW]	385	385	13
Stage 1	Output voltage of Panel A V_{SPVA}, [V]	5.45	5.45	5.45
	Output voltage of Panel B V_{SPVB}, [V]	3	3	5.45
	Bus voltage V_{bus}, [V]	8.45	8.45	10.9
	Bus current I_{bus}, [mA]	130	130	3
	Output power P_{bus}, [mW]	1095	1095	31
	Efficiency η_{MPPT}, [%]	92.2	93.1	80
Stage 2	Battery voltage V_{bat}, [V]	8.12	8.12	8.12
	Charging current $I_{charging}$, [mA]	130	130	0
	BCR power loss P_{loss}, [mW]	43	43	0
	Efficiency η_{BCR}, [%]	96	96	0

Table 7.2: Results of the test of the series configuration of two SPV1040 MPPT controllers followed by a MPC73213 linear BCR

In this test, the threshold voltage of the controllers is set to 5.5V.
The maximum power consumed P_{BCR}, power loss, P_{loss} and the worst BCR efficiency, η_{MCP}

are computed based on the bus voltage, 11V, the lowest battery voltage, 7.8V, and the charge current, 130mA:

$$P_{BCR} = 11 * 130 = 1430 \text{ mW}$$
$$P_{loss} = (11 - 7.8) * 130 = 416 \text{ mW}$$
$$\eta_{MCP} = \frac{P_{out}}{P_{in}} = \frac{7.8 * 130}{11 * 130} = 71\%$$

As the maximum power consumed is lower than the maximum power that can be harvested from the solar panels and that the output current is lower than the current at MPP of each panel, both SPV1040 are operational.
Under full irradiance of both panels, as the maximum power of panel B is lower than half of the power consumed, it is seen that the output voltage of the controller associated is reduced to 3V and that panel B operates at MPP.

Hence, panel A has to take care of the remaining power asked by the battery charger.
It can be seen that the output voltage of the SPV1040 associated is nearly at the threshold voltage. The imprecision comes from the potentiometer resolution.
The efficiency of the series configuration of the SPV1040 is measured with the bus power divided by the sum of the input power generated by the panels. As expected from the datasheet, an efficiency between 90% and 95% is obtained.
The efficiency of two SPV1040 in series is in the same range as the efficiency of a single chip.

It can be noticed to the BCR charges the battery with the programmed current, which is 130mA as expected.
As the bus voltage is close to the battery voltage, the efficiency of the BCR is quite high.
If a panel with a higher MPP than the panel B was chosen, the bus voltage would be increased and the efficiency of the BCR would decrease accordingly.

As panel A is inclined, although its I-V curve changed, the SPV1040 associated changes the panel's operating point in order to get the same output power.
For an inclination of 45°, it can be seen that the maximum power of panel A is still higher than the consumption of the BCR.
However, when the inclination is such that the maximum power of the panel is below the consumption of the BCR, the bus voltage drops and the battery charger enters idle mode and stops the charge of the battery.

The MPP of each panel is here different than their MPP in space conditions but the work principle and efficiencies are ensured. Based on these results, a theoretical approach of a series configuration of 3 and 5 MPPT can be discussed.

One might then be able to answer the question of how many controllers to use and how to connect them with the solar panels.

7.1.1 Two MPPT controllers in series

This architecture design uses 2 MPPT boost converters to control the 5 solar panels. The controllers are in series and followed by the linear battery charger MCP73213, cfr. Figure 7.3.

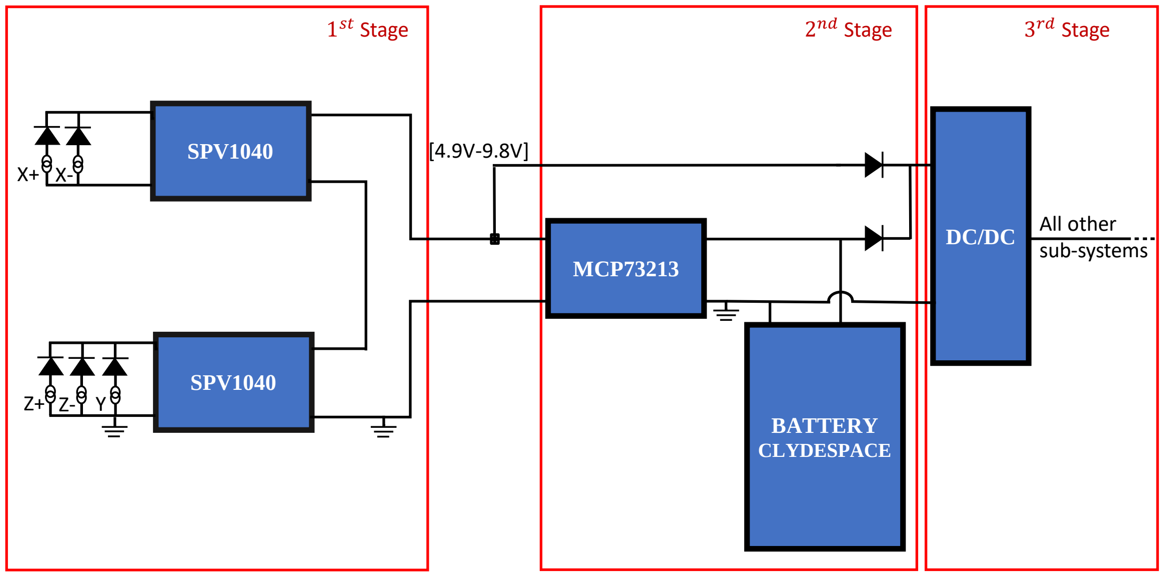

Figure 7.3: Architecture design of 2 MPPT boost controllers in series in front of a linear battery charger

In this configuration the first boost controller is fed by 3 solar panels, Y, Z+ and Z- in parallel. As Z+ and Z- are on opposite side, both cannot be directed to the sun simultaneously. As the Albedo effect and the Earth radiation contributes for the low infrared spectrum, their energy cannot be harvested by a solar panel[26]. Therefore, when two opposite side solar panels are in parallel, only one panel contributes to the solar input power.
From the maximum rating of the SPV1040, connecting several panel in parallel as input to the controller is not a problem. The maximum current of 1.8A cannot be reached by two panels.

The problem of the parallel connection of the solar panel is that both cannot operate at the MPP simultaneously if they have different I-V curve.
The SPV1040 will still act to get the maximum input power, and therefore the operating point of the panel with the higher MPP will be reached.

The worst case scenario occurs when one solar panel is inclined by α=67.5°compared to the sun, and the other one at β=22.5°, as represented in Figure 7.4.

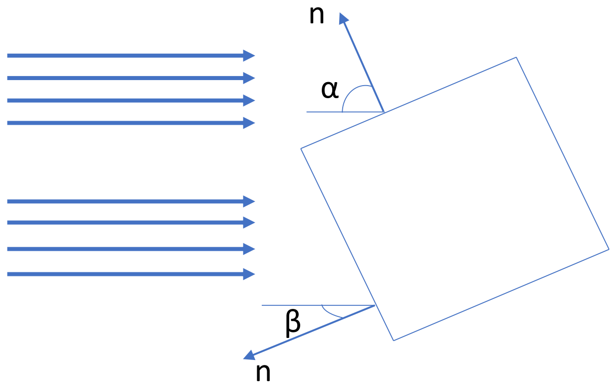

Figure 7.4: General representation of an insolation of only two solar panels of the cube

If the difference in inclination angles, $\alpha - \beta$, is higher than 45°, the power harvested by one panel becomes negligible. A lower inclination angle difference leads to nearly similar I-V curves and MPP.

In this scenario, one panel receives a normal relative insolation G=cos(22.45°)=0.92, i.e. 1263W/m^2, and the other one G= cos(67.5°)=0.38, i.e. 523.2 W/m^2.

The same matlab script as previously is used to simulate the power curve of OUFTI-2's solar panel under these insolations, at 55°C. Those graphs can be seen in Figures 7.5(a) and 7.5(b).

It can be seen that the voltage of maximum power for the more illuminated panel is 4.12V for a maximum power of 1717mW, while the MPP of the other panel is located at 4.39V and is equal to 760mW.

As the SPV1040 algorithm tracks the maximum power, it locates the operating point of both panels at 4.12V.
This corresponds to a power of 730mW. Hence only 30mW are lost in this configuration.

As only one panel is illuminated, the voltage of the bus drops to V_{lim}, the limitation voltage of only one SPV1040. At this moment, the battery charger is no more active, but the power consumption of the satellite is still ensured, since the maximum power of one panel is higher than the satellite's consumption (cfr. chapter 10).

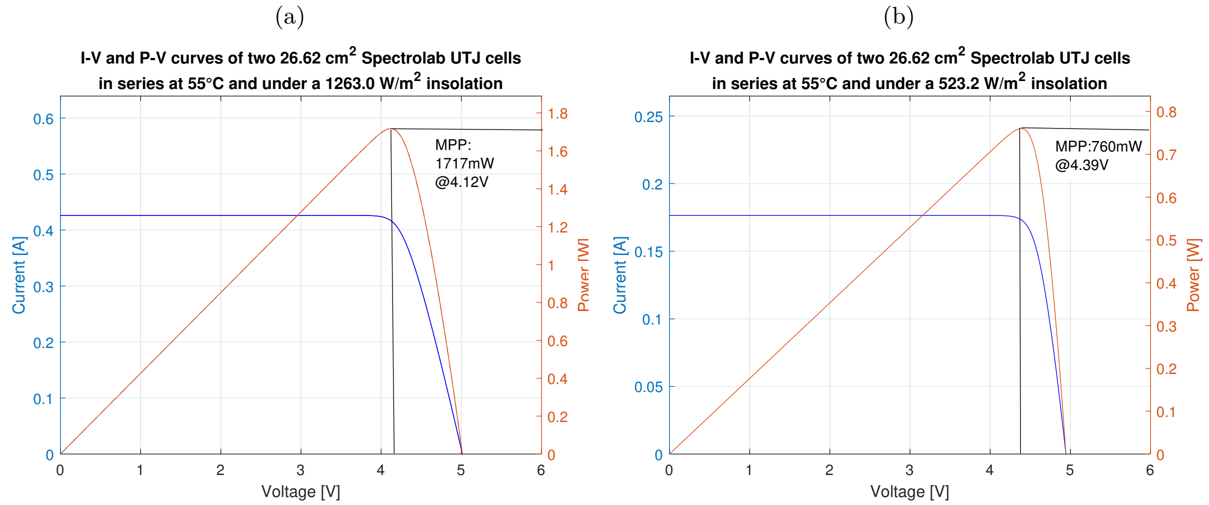

Figure 7.5: (a)Power-Voltage and Current-Voltage curves of two 26.62 cm^2 `Spectrolab` cells under relative insolations, G, of 0.92 at 28 °C (b)Power-Voltage and Current-Voltage curves of two 26.62 cm^2 `Spectrolab` cells under relative insolations, G, of 0.38 at 28 °C

This scenario is however seldom since the satellite spins around itself.

When the two SPV1040 are active, the bus voltage rises to twice the limitation voltage. In order to reduce the loss of the linear battery charger, the threshold voltage of each MPPT controller should be set to 4.9V. Setting the threshold to lower values would prevent the MPP of the solar panel to be reached.
In this way, the power loss in the battery charger is at most:

$$P_{loss}=(V_{bus}-V_{bat})*I_{charging}=(9.8-7.8)*0.130=260 \text{ mW}$$

Hence in this configuration, the maximum power is get out of the cell and the battery charger can operate most of the time. The BCR cannot operate only when just one side is illuminated and when the power consumption of the satellite is higher than the maximum power of the panels.

7.1.2 Three MPPT controllers in series

In this architecture, an additional boost controller is used, with the Y solar panel as input.
The advantage of this architecture compared to the previous is the separation of the Y and Z solar panels to a specific controller for each. Both panels are ensured to operate at the maximum power point even under different insolation conditions.
However, some drawbacks balances the gain of input power.
Firstly, as for the previous architecture, this configuration is not able to supply the battery charger when only one side of the satellite is illuminated.

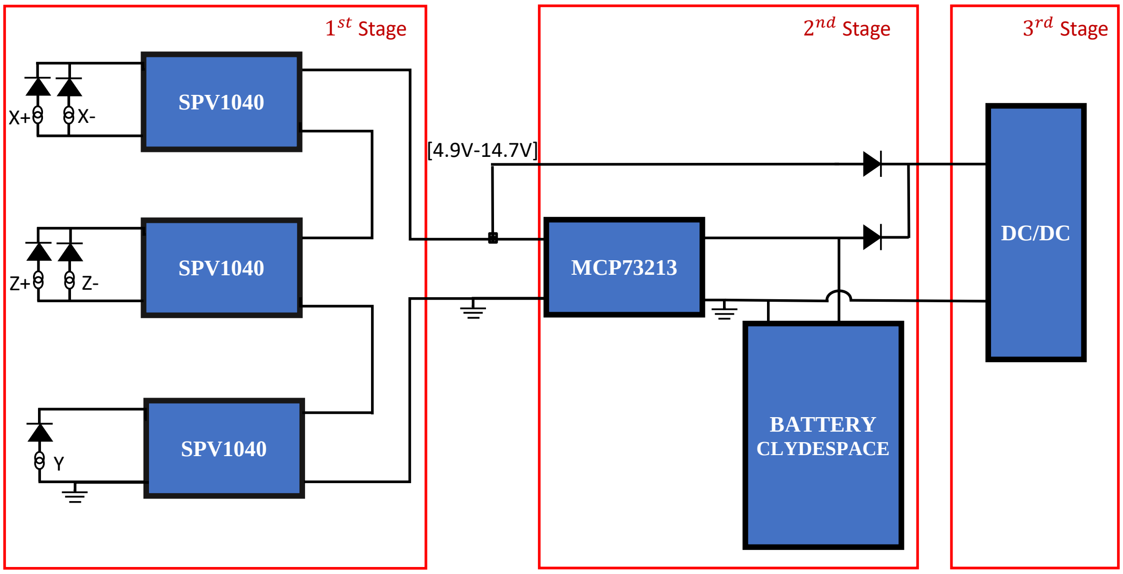

Figure 7.6: Architecture design of a serial connection of 3 MPPT boost controller in front of a linear charger controller

Secondly, the topology of the 3 MPPT controllers in series induces a higher bus voltage than the previous architecture, up to 14.7V if V_{lim} is kept at 4.9V.
The maximum power loss of the linear charger with a 130mA charging current is then

$$P_{loss} = (14.7 - 7.8) * 130 = 897 \text{ mW}$$

This corresponds to an efficiency of $\frac{7.8*130}{14.7*130} = 53\%$.
Hence this configuration only increases the bus voltage and the power losses for a negligible gain of 30mW.

7.1.3 Five MPPT controllers in series

This architecture dedicates a MPPT controller per solar panel. As their number is odd, only a connection in series of all controller is feasible, as shown in Figure 7.7.

Although the number of controller in series is higher than the solution with 3 MPPT controllers, the voltage of the bus stays the same. As opposite sides solar panels cannot produce power simultaneously, the controller corresponding to the shaded panel will not contribute to the bus voltage. The input power and the power loss in the battery charger is then the same than the 3 controllers in series solution.
This solution presents the same power characteristics as the previous one.

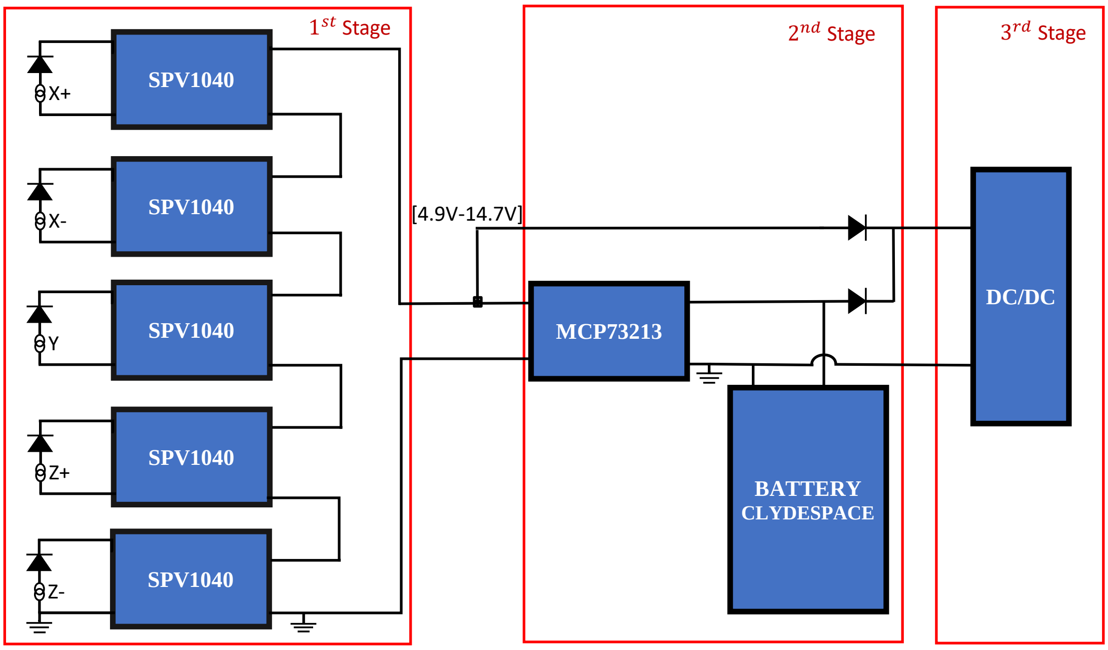

Figure 7.7: Architecture design of a serial connection of 5 MPPT boost controller in front of a linear charger controller

However, as the number of controller increases, so does the risk of failure.

7.1.4 Conclusion of the series configurations

From the test of the series configurations and the linear battery charger, the configuration with only 2 SPV1040 MPPT controllers presents the lower voltage bus, power dissipation in the battery charger and is the most reliable.

7.2 Cascade connection of a MPPT boost controller and a boost charger controller

The second architecture design to be tested is composed of a single SPV1040 as first stage then followed by a boost charger as second stage. The main goal of this architecture is to avoid a serial connection of the SPV1040 controllers. This design is represented in Figure 7.8. The first stage consists of 5 MPPT boost controllers SPV1040 in parallel. The choice of one for every solar panel is made to ensure that the maximum power point of each solar panel is reached when illuminated.
Although a controller can handle 2 opposite side panels in parallel as input, a failure of the controller deems then two panels unusable instead of one.

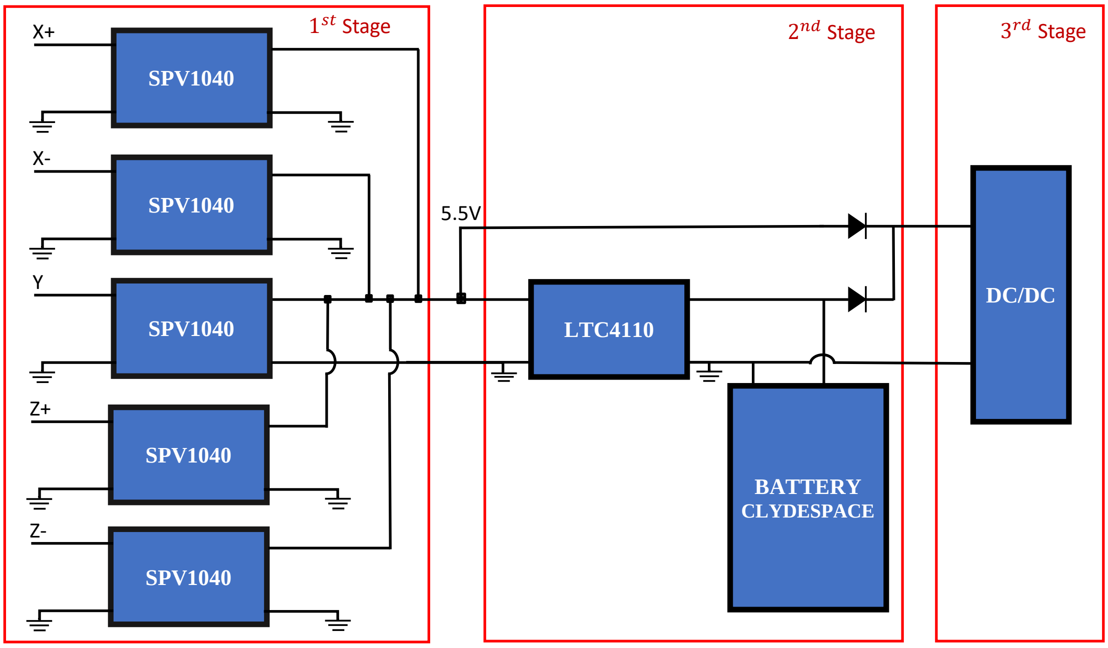

Figure 7.8: Architecture design of a cascade connection of a MPPT boost controller in front of a boost charger controller

The output of the controllers is connected to the input of the 2^{nd} stage: A boost battery charger able to step up a 5V input voltage to the battery voltage with a constant current constant voltage charge method.
Hence, the output threshold of the SPV1040 controllers should be fixed to the maximum in order to be able to supply the battery boost charger.
The LTC4110 *Battery Backup System Manager* from Linear Technology fits all the requirements[27].
Diodes ensure the battery is charged by the second stage and not the first one.

This configuration however rises one uncertainty that must be analysed, the consideration of the behaviour of the controller of each stage. It must be ensured that the system will not collapse due to one controller trying to force the other. This is tested in the next section.

7.2.1 Test of the management of the 2 controllers

To analyse the behaviour of the two controllers, each of them is analysed separately.
The MPPT boost controller was already analysed in Chapter 5.
A parallel connection of the MPPT controllers fixes the output voltage of the SPV1040. Hence, all controllers have an output voltage equal to the threshold voltage.

The second controller is the LTC4110, a PWM flyback charger with constant current constant

voltage charge operation.
The duty cycle of this controller is adjusted in order to keep a constant output current, which value is programmed in the controller. When the battery voltage is close to its maximum, the duty cycle is now controlled to maintain the output voltage while reducing the current, until the charge is complete.

This controller needs a certain amount of power to provide the constant current, constant voltage operation, which is function of the programmed charging current and the battery voltage.
As the battery voltage varies between 7.8 and 8.4V and the charge current is fixed to 130mA, the power consumption varies between 1014mW and 1092mW.

If the maximum power of the solar panels is higher than the sum of the BCR's consumption and the other sub-systems' consumption, then the bus voltage is fixed at the threshold voltage of the SPV1040, as seen in chapter 5. Then, both the BCR and the satellite are supplied by the solar panels. If the satellite consumes more power, i.e. when a transmission is operated, and that the solar panels do not produce enough power, the voltage of the bus drops. As the minimum input voltage of the LTC4110 is 5V, the second controller shuts down and the battery discharges into the satellite.

The evaluation board of the LTC4110, called DC1259A, has been ordered to test the chip.

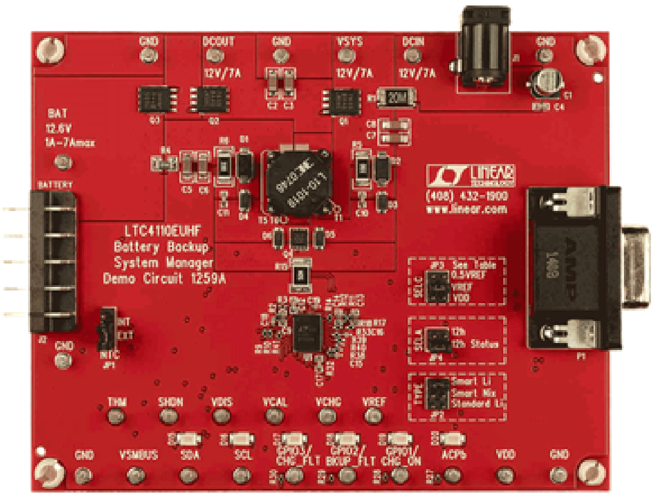

Figure 7.9: DC1259A: Evaluation board of the LTC4110 analog device battery backup system

As such, the board is designed for a 12V DC input and a charging current of 1A [28]. The controller enters the back-up mode, i.e. when the battery charges the load instead of the DC supply, when the DC supply drops below 11V.

However by replacing a few components on the board, the back-up voltage and the charging current can be tuned to respectively 5V and 130mA.
In this configuration the charge of the battery can be carried with an input voltage up to 5V.
Jumpers allowing to select the type of battery are set up for a 2sp1 Lithium Polymer battery.

Similarly to the test of the series configuration, the two controllers are tested on a cloudless day. As the power consumption of the battery charge is lower than the 1826.8mW maximum power of the solar cells, the SPV1040 are operational.
Figure 7.10 is a picture of the test set-up.

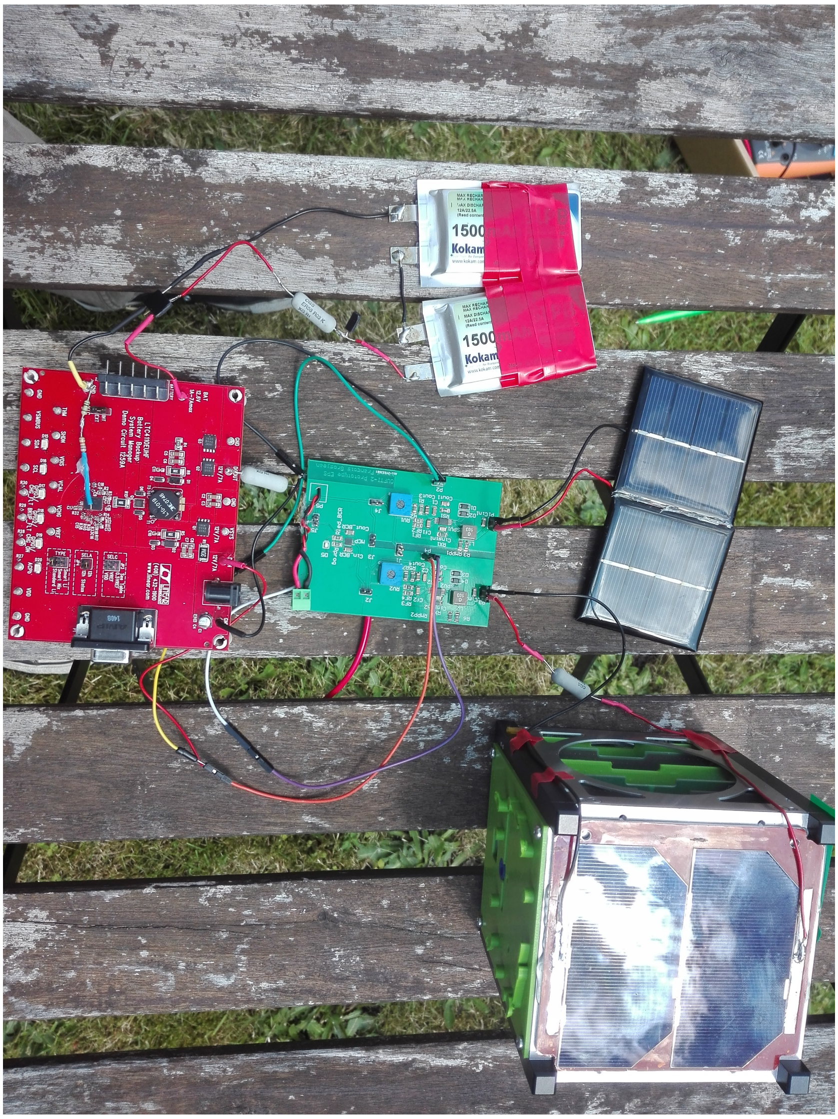

Figure 7.10: Picture of the test set-up of the parallel configuration

The solar panels and the battery are connected to the two SPV1040 controllers of the homemade development board in a parallel configuration. The LTC4110 is connected to the output of the MPPT controllers. Panel A and B are the same as for the series configuration test.
The voltages, currents and power of each stage are measured, and the efficiencies are then computed.
The results are shown in Table 7.3.

Stages	Parameters	Full irradiation on both panels	Panel A inclined by 45\degree	Panel B inclined by 90\degree
Panel A	Input voltage V_{inA}, [V]	4.8	4.7	5.2
	Input current I_{inA}, [mA]	223	185	3
	Input power P_{inA}, [mW]	1071	869	16
Panel B	Input voltage V_{inB}, [V]	2.8	2.7	5.2
	Input current I_{inB}, [mA]	45	74	0
	Input power P_{inB}, [mW]	127	201	0
Stage 1	MPPT output voltage V_{bus}, [V]	5.25	5.25	5.25
	Bus current I_{bus}, [mA]	207	204	2
	Output power P_{bus}, [mW]	1088	1070	11
	Efficiency η_{MPPT}, [%]	90.9	92.3	69
Stage 2	Battery voltage, V_{bat}, [V]	8.19	8.19	8.19
	Charging current $I_{charging}$, [mA]	128	128	0
	BCR input current I_{BCR}, [mA]	208	204	0
	Efficiency η_{BCR}, [%]	96	98	0

Table 7.3: Powers and efficiencies of the 1^{st} and 2^{nd} stages of the cascade connection of a SPV1040 MPPT controller and a LTC4110 BCR

It can be seen that when the BCR is activated, the charging current is nearly close to 130 mA. The 2mA difference can be due to the precision of the resistors chosen.

Under full irradiation of both panels, it can be seen that the input voltage of the panels are close to the MPP. The MPP are not reached since the chips cannot harvest more power than the power consumed.
In this configuration the efficiency of the SPV1040 controllers is found by dividing the sum of the harvested power by the bus power. The efficiency is still around 91%. The efficiency of the BCR is high, as expected from a switch-mode BCR, and is 96%.

When OUFTI-2's solar panel is inclined by 45 °, it can be seen that the voltage is still quite close to the maximum power voltage but the power harvested is reduced. This is due to the lower I-V curve of the panel, since its receives less insolation.
As the insolation of panel B does not change, its MPP remains the same.
However, as less power is produced by panel A, the operating point of panel B can be adjusted closer to its MPP.

When the inclination of one panel is such that the sum of the panel's maximum power is lower than the consumption of the BCR, the voltage bus drops below the back-up voltage of the LTC4110 and the charge is stopped.

7.3 Efficiency of the TSP62130 step down converters for every solution

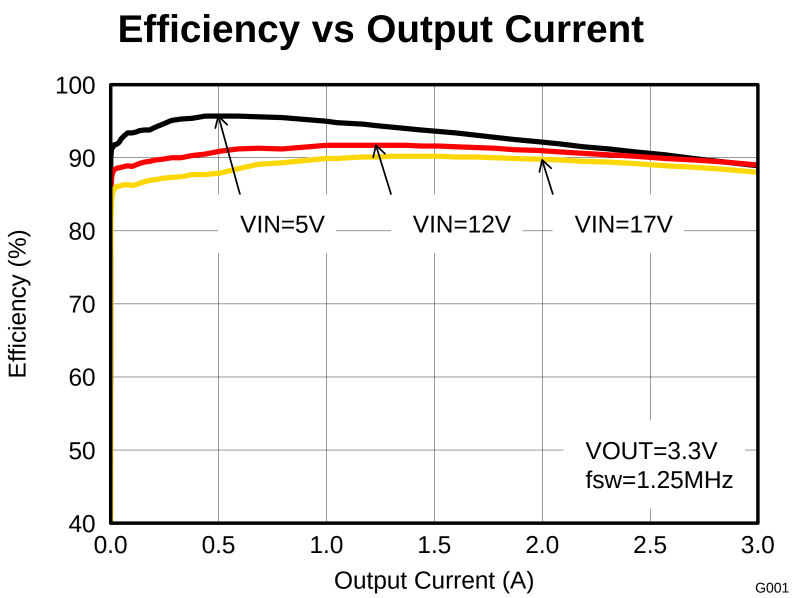

Figure 7.11: Efficiency of the step down converter TPS62130 from Texas instrument as a function of the output current, for input voltages of 5V, 12V and 17V

Obviously, the efficiency of a step down converter with a fix output voltage is function of its input voltage. As every solution design leads to different bus voltages, a different power efficiency of the step down converters can occur from a design to another.

Figure 7.11 from the datasheet of the converter[24], shows the evolution of the efficiency of the converter based on its output current for different input voltages.

The output current is function of the operation mode of the satellite.
As can be seen in the Power Budget, for an operation mode of the satellite without any transmission, the current of the bus is estimated to be 600mA.
The estimated bus voltage of every solution designs of the series configuration are compared in order to measure their converters efficiency.

	Serial connection 5 MPPT	Serial connection 3 MPPT	Serial connection 2 MPPT	Parallel connection 5MPPT
Maximum voltage bus, V_{Bus}	24.5V	14.7V	9.8V	5.5
TPS62130 power efficiency, η_{TPS}	<90%	90%	91%	95%

Table 7.4: Efficiency of the TPS62130 for different architecture design

7.4 Reliability analysis

Reliability is a fundamental criteria for a space mission.
Problems must be avoided, and if one still occurs, the risk associated must be minimised.
This section has for goal to analyse qualitatively the reliability and risk of every architecture designs.

For the parallel configuration of SPV1040, as each solar panel has its own controller and that the 5 controllers are connected in parallel, even if a problem occurs in one MPPT controller, the others can still operate normally. The power harvested is reduced by one fifth of the original harvest.
If a problem short-circuit the terminal of one SPV1040, all the other controllers are lost as well.

Considering the 2^{nd}stage, if the LTC4110 encounters a problem, the battery is not charged anymore.
As explained in the Power budget, Chapter 10.1, the consumption of the satellite when the payload is active is higher than the power that can be harvested instantaneously from the solar

panels. Hence, the battery is essential to supply the consumption of the payload. Losing the battery charger then leads to a loss of the mission.

Considering a serial connection of the MPPT boost controllers, an error in one controller impacts all other controllers, which leads to a total loss of all power harvest during the mission. The more the boost controllers in series, the higher the risk.
An error at this stage is fatal since no more power can be harvested.
Only the battery is then able to power the satellite until it is discharged.
The linear battery charger related to this architecture is however very robust.

To conclude, a parallel connection of the SPV1040 controllers allows a lower loss of power than the series connection in case of failure of one controller. However as the architecture using the parallel configuration uses 5 MPPT, the probability of a failure is higher than for the architecture using a series connection of only 2 MPPT.
Furthermore, the linear battery charger with its simplicity is far more reliable than the switching mode BCR.

7.5 Summary

Table 7.5 gathers the conclusion from each section of the test chapter. The power efficiency of each stage of the architectures, the complexity and reliability of each design are the parameters of the comparison.

Comparison Parameters	Series connection of 2 MPPT	Series connection of 3 MPPT	Series connection of 5 MPPT	Parallel connection of 5MPPT
SPV1040 Power efficiency	92.1%	92.1%	92.1%	91.6%
TPS62130 Power efficiency	91%	90%	<90%	95%
Worst case BCR Power efficiency	71%	51%	51%	96%
Total efficiency	68.5%	45%	<45%	82%
Complexity	low	low	low	high
Reliability	high	medium	medium	low

Table 7.5: Comparison table of the four architecture designs discussed

For the BCR efficiency, the worst case scenario, i.e. the lowest battery voltage and highest bus voltage, is always stored in the table.
As the efficiencies of the SPV1040 measured during the test depended on the inclination of the panels, a mean value is taken.

For the 3 and 5 MPPT in series configuration, only the theoretical efficiencies are stored.

It can be seen that the higher efficiency is obtained when the LTC4110 is used in the architecture design. The lower voltage of this architecture bus leads to a higher efficiency of the TSP62130 converters. In the other hand, a better reliability is achieved with a serial connection of two SPV1040 and a MCP73213.

Adding more than two SPV1040 boost controllers in series only decreases the efficiency of the battery charger and the TPS62130 converters. A parallel configuration of the SPV1040 or a connection in series of 2 are then the best options.
In order to choose between one or the other, the maximum power loss of the battery chargers is a key parameter.
The maximum power loss of the linear battery charger MCP73213 in the series configuration of two MPPT controllers is 234mW. The maximum loss of the switch-mode battery charger is computed on the tested efficiency of 96% and is found to be 43mW.

In the power budget, chapter 10 it is ensure that the payload can be used even with the maximum power losses of the MCP73213 BCR.
The power budget also discusses the duration of the charge of the battery when using the MCP73213 BCR or the LTC4110 BCR. As the losses of the LTC4110 are lower, for a same consumption, the charging current could be increased to 180mA.
If the battery has reached its maximal DoD of 20%, the MCP73213 with 130mA, needs 6 standard orbits to fully recharge the battery, while the LTC4110 can recharge it in 3 orbits, in the same conditions.

It is also shown that in a worst case orbit, in both cases the payload can be activated more than 6 minutes and 12 seconds per orbit and that the battery can be recharged after the operation.

Based on this power analysis, as both can operate the satellite, the more reliable and simple solution is preferable.
Thus, the final architecture chosen is the configuration of 2 SPV1040 MPPT controllers in series followed by a dual cell linear charger MCP73213.

8 Power path overview

In this section the power path of the semi-regulated bus is tested for both battery chargers and for a series or parallel connection of the MPPT controllers.
The aim is to ensure that the battery is charged only by the BCR and that the battery discharges only when solar panels cannot provide enough power to supply the satellite.

The equivalent load, R to simulate the power consumption P_{cons}, of the other sub-systems of the satellite is function of the operations of the satellite and the bus voltage, V_{bus}:

$$R = \frac{V_{bus}^2}{P_{cons}} \tag{8.1}$$

Table 8.1 indicates which load to chose to simulate each power consumption scenario based on two different bus voltages. The 5.5V and 9.8V voltages of the table represent respectively the bus voltage of the series and parallel configuration.

The equivalent loads have been chosen to simulate 3 particular power consumptions. A first power consumption of 250mW to ensure the stability of the set-up. The second power consumption of 1055mW corresponds to the consumption of the satellite during a standard orbit, i.e. without any transmissions, and without the battery charger's consumption. The last power consumption of 6000mW corresponds to an estimation of the power consumed by the satellite when a transmission is operated (cfr. chapter 10.1).

		Power consumption P_{cons}, [mW]		
		250	1055	6000
Bus voltage V_{bus}, [V]	5.5	121Ω	28Ω	4Ω
	9.8	384Ω	91Ω	16Ω

Table 8.1: Load simulating the consumption of the rest of the satellite based on the bus voltage

As the behaviour of the solar panels and the MPPT have already been tested and in order to avoid dependence on cloudless day, an external power supply was used to simulate the 1^{st} stage of the parallel and series configuration.
The voltage of the power supply is set to the bus voltage and the current limit is set such as the maximum power from the power supply is equal to the maximum power harvested from the panels. This power is found to be 2352mW in the power budget section.
Hence, the current limit is set to 427mA for a bus voltage at 5.5V, and 237mA for the 9.8V bus voltage.

The following materials were used for the test:

- DC Power supply CSI1802X [0-18]V and [0-2]A
- Four multimeters TENMA 72-7730A
- Two 30mΩsense current resistors, 7W, from CGS
- One decade resistor DB59Dekabox of 111kΩand a resolution of 1Ω
- Two 1500mAh LiPo battery cells in series
- One schottky diode of 0.3V forward bias
- DC1259 Development board of the LTC4110 BCR

8.1 Series configuration

A representation of the test set-up is shown in Figure 8.1.

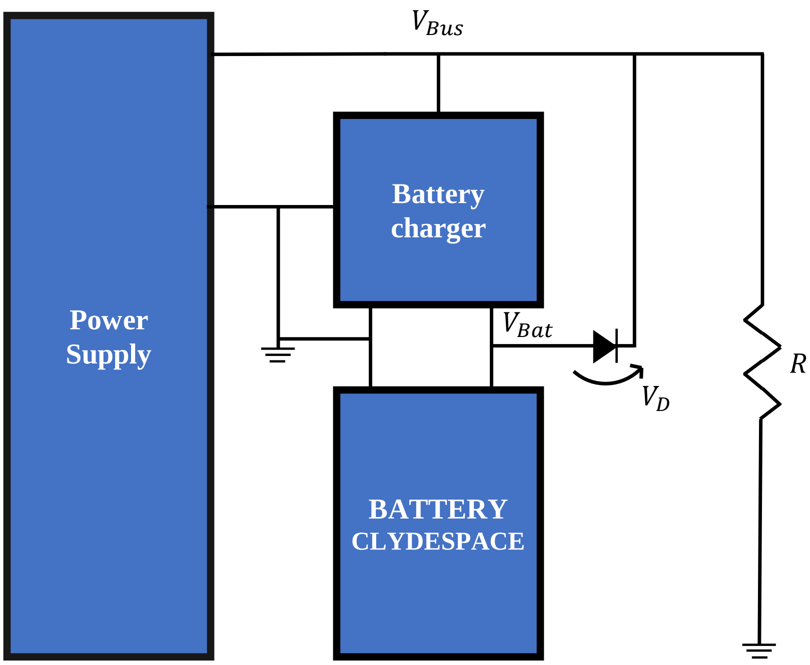

Figure 8.1: Representation of the test set-up of the power path simulation of the series configuration of 2 MPPT controllers

In this set up, considering a battery voltage of 8.11V, the bus voltage is either 9.8V when the maximum power harvested is higher than the power consumed, or 7.6V when the battery discharges through the diode.

For a 9.8V voltage bus, the total power consumption of the linear BCR, P_{BCR} is simply the product of the bus voltage V_{bus} and the charging current $I_{charging}$:

$$\begin{aligned} P_{BCR} &= V_{bus} * I_{charging} \\ &= 9.8 * 130 = 1274\text{mW} \end{aligned}$$

For the two first power consumptions of 250mW and 1055mW, the power requested by the load and the battery charger is lower than the maximum input power available. The bus voltage is still at 9.8V, the battery is charged with 130mA and the load consumes the power expected.
As the voltage of the bus is higher that the voltage of the battery, the diode is in reverse bias and no current is flowing from the battery to the load.

When the load is decreased to 16 Ω, the current limit stops the power supply and stops the charge of the battery. The voltage of the bus drops to the voltage of the battery, V_{bat}, minus the forward bias of the diode, V_D. A voltage of 7.6V was measured. The current drawn from the battery is measured to 165mA.

In this mode, the power harvest from the solar panel does not stop. As the battery discharges in the load, the equivalent power consumption seen by the MPPT controllers is now lower than the maximum power of the solar panels. The SPV1040 controllers can thus operate again.
When the load is increased back to 83Ω, the bus voltage rises to 9.8V and the battery no longer discharges.

From this test, it is now ensured that the battery is able to charge and discharge correctly through the semi -regulated bus.

8.2 Cascade configuration

A representation of the test set-up is shown in Figure 8.2.
In this set up, the bus voltage is either 5.5V when the maximum power harvested is higher than the power consumed, or 7.95V when the battery discharges.
The LTC4110 has the feature to implement its own power path through transistors and a digital control.

For the two first power consumptions of 250mW and 1055mW, the input currents are measured to be respectively 264mA and 405mA. As for the series configuration, the battery is charged and the load is supplied as long as the total power consumption is lower than the maximum power that can be provided.

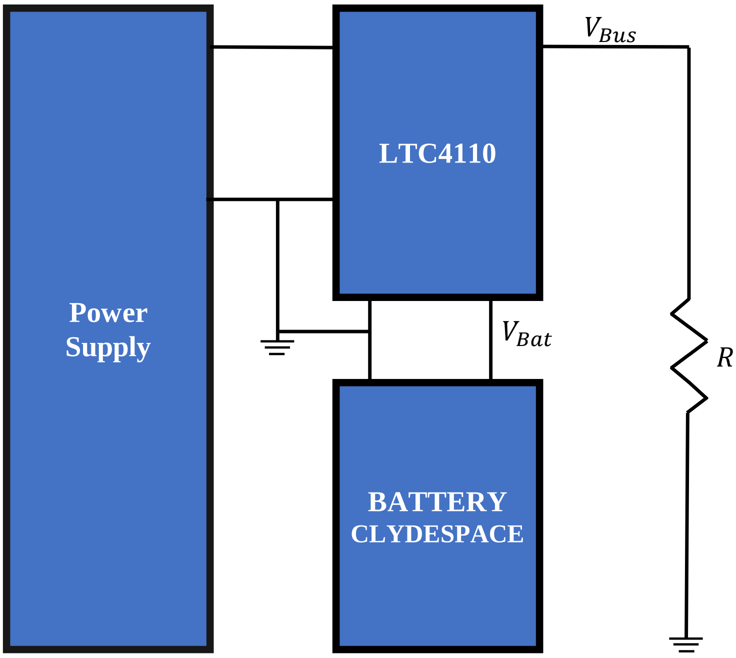

Figure 8.2: Representation of the test set-up of the power path simulation of the parallel configuration of 5 MPPT controllers

When the load decreases to 4Ω, the LTC4110 enters the back-up mode, the charge of the battery stops and the voltage of the bus rises to 7.95V.
The difference compared to the series configuration is that the power supply is totally disconnected from the load via the LTC4110.
Hence, even if the solar panels are illuminated no power can be harvested is the power consumption is higher than the maximum power of the panels.
This corroborate the decision of the series configuration architecture.

9 Prototype of the test board

9.1 Design of the prototype

In the case of the cascade solution, a development board of the LTC4110 already existed. However, although a development board for a single MPPT controllers SPV1040 exists, a homemade Printed Card Board (PCB) was needed to test two controllers in series.
The PCB allowed to understand the behaviour of two SPV1040 in series and to analyse the principle of the linear battery charge MCP73213 in a compact design.
Figure 9.1 is a high level representation of the functionality and connections of the board.

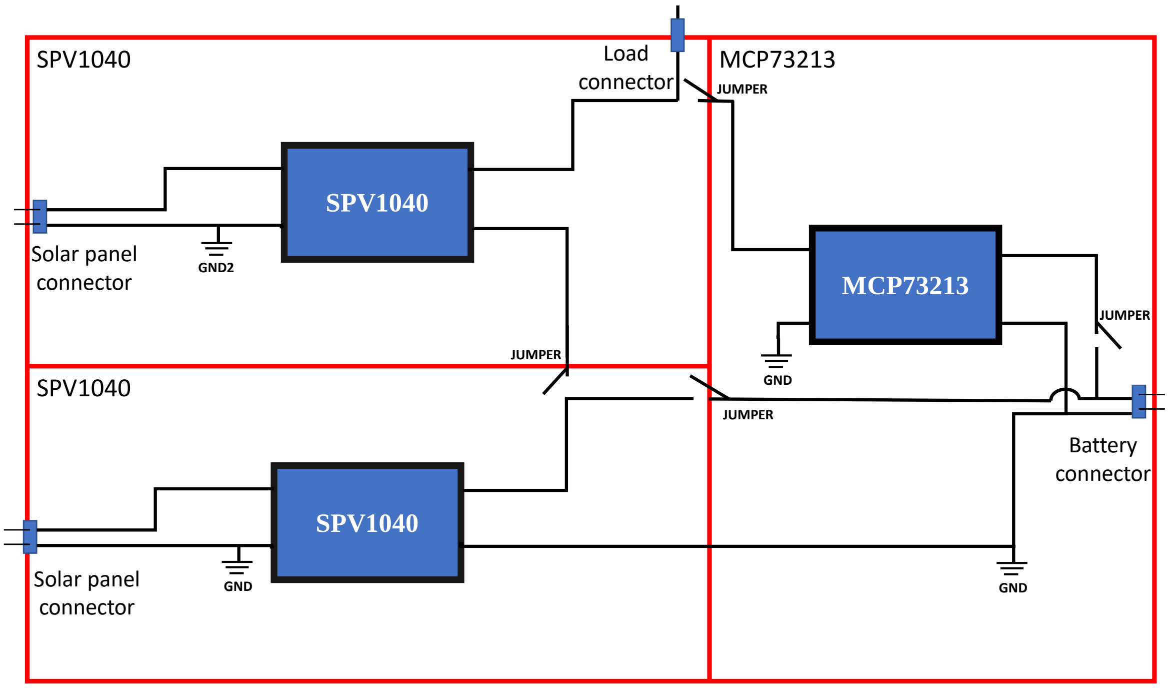

Figure 9.1: High level representation of the test board of two MPPT controllers in series and a linear battery charger

The board is split in 3 independent parts that can be connected together through jumpers, enabling every block to be tested independently.
The external components required by the SPV1040 and the MCP73213 are chosen as suggested in the application notes provided by the manufacturers [15] [29].

A potentiometer is placed in each SPV1040 block in order to be able to adjust their output voltage limit.

9.2 CAD layout & final board

The Computer Aided Design (CAD) program `Altium` has been used to edit the PCB of the board.
The final schematic design and PCB layout can be found in the appendix 13. A picture of the board after soldering of its component is shown in Figure 9.2.
Each block of the card was tested separately to ensure the quality of the soldering.

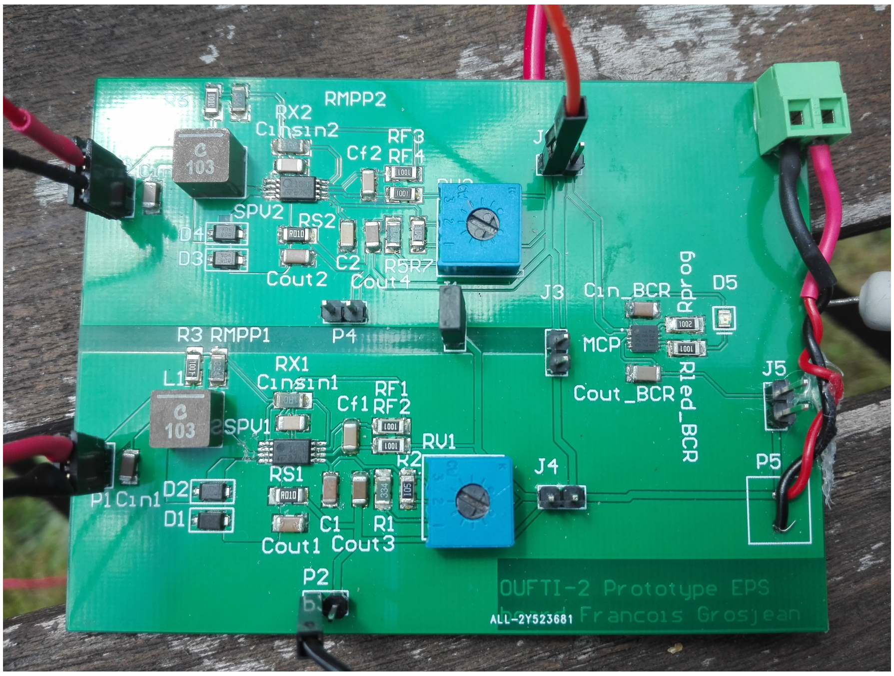

Figure 9.2: MPPT controller series connection prototype's picture

After this check, the card was ready to be used for the test review of the series and parallel configurations architecture.

10 Power Budget Discussion

The balance between power production and consumption is extremely important. The harvested power from the solar cells must be enough to supply all sub-systems of the satellite.
A power budget is the key to analyse such a power balance.

10.1 Power Budget Philosophy

The strategy used for the power budget of OUFTI-2 is to estimate the average power harvested from the solar panels during one orbit. This power is then compared with the consumption of all sub-systems in different operation modes over one orbit as well. The battery has the role of buffer to charge or discharge in order to balance the power budget.

The first operation mode of the satellite considered is the standard case. The minimum requirements for the satellite to be operational are considered, i.e. no transmissions from the D-STAR and AX.25 communication sub-systems.
If the power harvested is higher than the power consumed, a positive power margin is produced over an orbit. This margin can be used to charge the battery when needed.
The second operation mode is the transmission (Tx) mode. The duration of the activation of the transmissions and their effect on the power consumption of the satellite are analysed in this section.

10.1.1 Orbit model and power simulation

Since OUFTI-2 is deployed from the ISS, both object share a quite similar orbit at the start of the mission. Soon the CubeSat will start to fall due to air drag and will eventually burn in the atmosphere.

The orbit parameters of the ISS were used to simulate the trajectory of OUFTI-2. [30] A student license of the program `Systems Tool Kit (STK)`, a physics-based software package, was used to this end.
The orbit is found to last 92.88 minutes with an eclipse duration of 32.14 minutes in the worst case scenario.
Figures 10.1 represents the orbit of OUFTI-2 on the 28$^{\text{th}}$ February 2019 and its 3D representation in the `STK` environment.

The `STK` model of OUFTI-2 also allows to compute the effective area A_{eff} over an orbit. This area is the mean area, over one orbit, of solar panels illuminated by the sun, adjusted by the cosine of the angle of incidence of the sun to the solar panels.

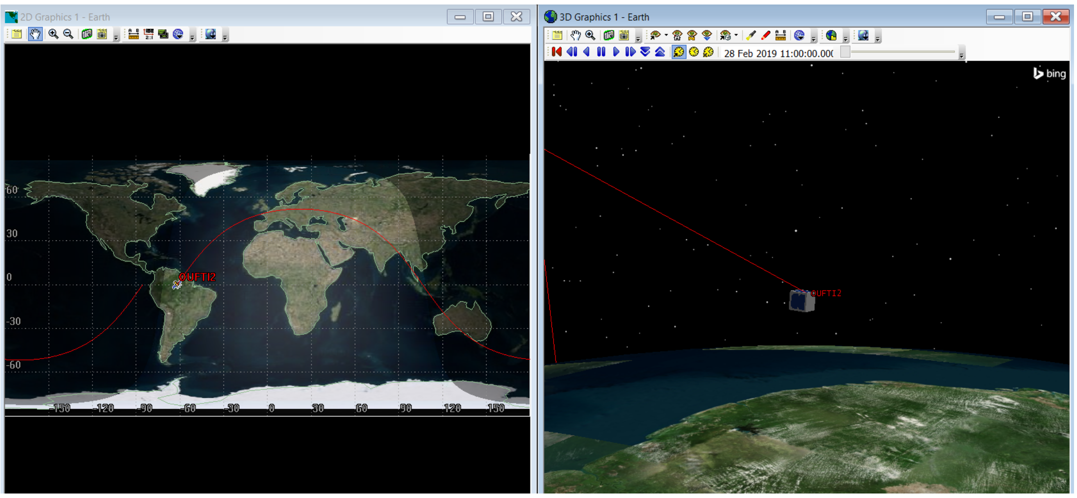

Figure 10.1: 2D and 3D views of OUFTI-2 orbit trajectory on STK starting from February 28, 2019 11:00:00

The same was done for the effective area of OUFTI-1, which was found to be 76.6 cm^2.[3] However, as the orbit trajectory of OUFTI-2 changes from the one taken by OUFTI-1, a simple linear transformation from the effective area of OUFTI-1 to the effective are of OUFTI-2 might be too simplistic.

A new 3D model for OUFTI-2 was designed with the help of the program `Sketch-up`. Figure 10.2 shows the cubesat model with its solar panels.

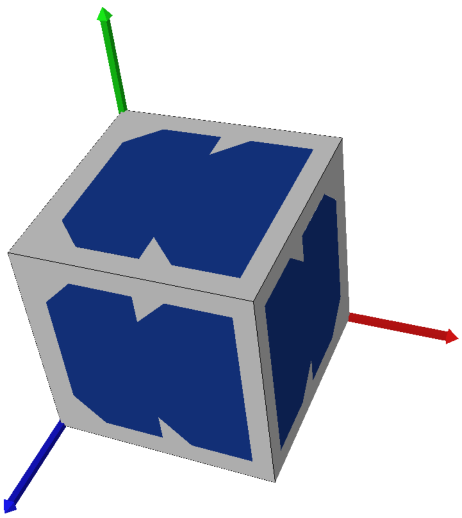

Figure 10.2: 3D model of OUFTI-2 via `Sketch-up`

An additional ancillory file establishes which components of the model are solar panels for the

STK simulation to work with. This file can be found in appendix 13.

A report with the total effective area of the solar panels at every time step is given by `STK`. This report can be exported to `Matlab`, where the mean area over an orbit is then computed. The script `Aeff_calc` in appendix 13 implementing this code, outputs an effective area of 66.67 cm^2.

10.1.2 Available Power

As the MMPT controllers enables the solar panels to operate at MPP, an estimation of the available power produced by the solar panels at a given time, is given by:

$$P_{in} = \eta_{PV} \eta_{MPPT} A_{eff} C_s$$

where :

- η_{PV} is the efficiency of the solar cells
- η_{MPPT} is the efficiency of MPPT controller
- A_{eff} is the effective area of solar panels onto which the solar rays are projected
- C_s is the solar constant

From section 7, the mean efficiency of the MPPT controller SPV1040, η_{MPPT} is found to be 92.5%.

The solar constant is the solar energy available at the top of the atmosphere. Depending on the distance between the Sun and the Earth, the solar constant varies from 132.1 to 141.3 mW/cm^2, with a mean value of 135.8 mW/cm^2 [3].

As the CubeSat is deployed from the ISS, it will take only a few months for it to decompose in the atmosphere. Hence, the efficiency of the solar cells is considered to remain close to the one at BoL, i.e. 28.3% [7].

The instantaneous available power generated by the solar panels of the satellite can then be estimated for a mean solar constant $C_{s_{mean}}$:

$$\begin{aligned} P_{in} &= \eta_{PV} \eta_{MPPT} A_{eff} C_{s_{mean}} \\ &= 0.283 * 0.925 * 66.63 * 135.8 = 2375 \text{mW} \end{aligned}$$

The worst case scenario corresponds to the orbit with the longest eclipse duration: 32.14 minutes. The mean instantaneous available power is then multiplied by the percentage of sun

of the orbit, 65% in order to get the power harvested over one orbit.
Table 10.1 gathers the estimated power harvested for a minimum, mean and maximum solar constant over an orbit:

	Solar constant in [mw/cm^2]		
	C_{min}=132.1	C_{mean}=135.8	C_{max}=141.3
Instantaneous power harvested [mW]	2295	2375	2455
Power harvested over an orbit [mW]	1501	1553	1605

Table 10.1: Estimated harvested power by OUFTI-2 on the worst case orbit for a minimal, mean and maximum solar constant

The mean power that can be harvested over an orbit is found to be 1553 mW.

10.1.3 Power consumption

To estimate the consumption of the satellite, the architecture of the series configuration of 2 MPPT controllers is chosen.

As every sub-system is powered with steady voltages, their power consumption is based on the current they draw.
The currents used in this section are first estimations. More accurate measurements must be done when every sub-systems is finalised.

In order to compare the power consumptions with the average power harvested, the percentage of activation time of every sub-system is taken into account.
All sub-systems of OUFTI-2 were introduced in section 2.
The efficiency η_{DCDC}, of the four DC/DC converters are also taken into account.
From the manufacturer [24], the efficiency η_{DCDC} is estimated at 91% for a input voltage of 9.8V to an output voltage of 5V or 3.3V.
For an output voltage of 1.8V, the efficiency drops to 82%.

Table 10.2 summarises the power consumption of every sub-systems in a standard operation mode.
In this mode, the reception communication module, the OBC, the RAD and the IMU sub-systems are always activated.
Concerning the BCN and the THER modules, they both have two different modes.
The BCN is always emitting at 12 words per minute, however half of the time, bursts are send.
The consumption of the the BCN during each mode has been measured on the development board. Both consumptions are taken into account in Table 10.2.

Sub-systems	Power consumption P_{inst} [mW]	Activation time percentage [%]	Orbital power consumption ,P_i [mW]
AX.25 RX	163	100	163
AX.25 TX	4533	0	0
D-STAR	4533	0	0
BCN	88	50	44
BCN BURST	604	50	302
OBC	458	100	458
THER CST	110	100	110
THER ON	220	35	76
RAD	18	100	18
IMU	18	100	18
Bus power loss	41	100	41

Power Budget [mW]

Instantaneous $P_{Harvested}$	2375
Orbital $P_{Harvested}$	1553
P_{Cons}=$\Sigma_i P_i$	1231
Power margin ΔP	**322**

Table 10.2: Standard mode operation: Power consumption of every sub-system and its activation percentage over an orbit

The THER module consists of the integrated heaters of the `clydespace` battery. The module has a quiescent consumption, called THER CST, of 100mW even with the heaters disabled.[8]. Turning on the heaters consumes 200mW and is done as soon as the battery temperature drops below 1°C. No thermal design and simulation of OUFTI-2's mission have been carried out yet. A worst case approach is then followed to estimate the temperature of the battery. As the temperature drop only occurs during eclipses, the worst case consumption of the module is for the longest eclipse, i.e. 32.14 minutes.

The losses through diodes, protection components and measurement resistances are computed with the bus current. This current is based on the power requested by the sub-systems and the voltage of the bus. These components have not been chosen yet so typical resistance values and forward voltages are chosen.
The table with the details can be found in appendix 13.

The power margin, ΔP, is positive and represents 20.8% of the power harvested over an orbit. This margin means that more power can be harvested than the satellite consumes. The extra power can be used to charge the battery.

From this power margin, it is now possible to compute the battery consumption during charge, based on the charge current.

In order for the solar panel to operate as close as possible to their MPP, the charging current of the battery should be set based on the remaining power available:

$$P_{bat}=P_{harv}-P_{cons} \tag{10.1}$$

where

- P_{bat} is the power consumed by the battery
- P_{harv} is the instantaneous power from the solar panels = 2375mW
- P_{cons} is the power consumed by the other sub-systems when the satellite is exposed to the sun, i.e. the heaters are not activated, and no transmissions are operated

From Table 10.2, P_{cons} can be computed and is 924 mW.

Hence,

$$P_{bat}=P_{harv}-P_{cons}=2375-924=1451 \text{ mW} \tag{10.2}$$

From this power available, the charging current can be computed.
The power consumed by the linear BCR is simply the bus voltage times the charging current. Considering the architecture design of two MPPT controllers in series, the bus voltage is 9.8V. The charging current able to maximise the power harvested from the solar panel is $\frac{1451}{9.8} \simeq 150$mA for a mean case.

However, as the MPPT controllers cannot operate when the consumption demand is higher than the maximum power it can produce, this charging current is a bit reduces to ensure the controller to operate in all conditions.
A value of 130mA is chosen as it is the lowest value that can be programmed for the MCP73213 linear BCR.

Now that a power margin is ensured for a standard operation mode and that the battery can be charged, other higher consuming operations based on the duration of the D-STAR and AX.25 transmissions can be discussed.
As both communications protocol cannot be used simultaneously, the peak instantaneous power consumption accounts for 5905mW, drawing a bus current of 586mA. This high current increases the bus power losses which must be taken into account when a transmission is activated.
The new power losses are computed similarly to the power losses, via the bus current, as can be seen in appendix 13.

Table 10.3 shows a scenario of a balanced power budget, i.e. when the total power harvested is equal to the power consumed over the orbit, in the case of a mean solar constant.

Sub-systems	Power consumption P_{inst} [mW]	Activation time percentage [%]	Orbital power consumption ,P_i [mW]
AX.25 RX	163	100	163
AX.25 TX	4533	3.33	138
D-STAR	4533	3.33	139
BCN	88	50	44
BCN BURST	604	50	302
OBC	458	100	458
THER CST	111	100	111
THER ON	222	35	76
RAD	18	100	18
IMU	18	100	18
Rx Bus power loss	41	93.33	39
Tx Bus power loss	345	6.66	23

Power Budget [mW]

P_{Cons}=$\Sigma_i P_i$	1553
$P_{Harvested}$	1553
Power margin ΔP	**0**

Table 10.3: Transmission mode operation: Power consumption of every sub-system and its activation percentage over an orbit

In this balanced operation mode, the D-STAR and AX.25 transmissions are used 6.66% of the orbit duration, i.e. 6 minutes and 12 seconds.
The power consumed by the satellite over the orbit is then equal to the total power harvested when the satellite is exposed to the sun.

Longer transmissions lead to a negative power margin, i.e. the battery is used more than they can be recharged over the orbit.
This is not a problem as long as the battery were sufficiently charged before the operation.
However, the next orbits have to operate in a standard mode to recharge the battery. The number of standard operation mode orbits needed to fully recharge the battery is then function of the length of the transmission.

10.2 Battery configuration and DoD scenarios

In order to increase the longevity of the LiPo cells, a maximum Depth of Discharge (DoD) of 20% is recommended by the manufacturer [8]. This corresponds to a discharge of 3330mW during one hour for the 10Wh `Clydespace` battery used in OUFTI-2.

As the minimum sun time of the orbit accounts for 60 minutes and 74 seconds and for a charging current of 130mA, the battery gain at least 131.6mAh over sunlight, i.e. 10% of the battery capacity. However, the energy consumed during the longest eclipse with no transmission is 1231mW*32.14min/60=659mWh. This corresponds to a DoD of 6.3% of the battery.
Hence, per orbit, if no transmissions are activated the battery can be recharged by 3.7%, in the worst case scenario.
Considering a maximum DoD of 20%, the battery will always be fully charged after 6 successive standard mode operation orbits.

If the LTC4110 BCR was used with a charging current of 180mA, the battery can be recharged by 14% in one orbit. Only 3 standard mode operation orbits would then be needed to charge the battery if it had reached 202% of DoD.

Different operation modes were simulated on an orbit timeline in order to visualise the DoD of the battery in Figure 10.3.
The charge of the battery is operated with the MCP73213 in these timelines.

The first scenario represents a standard operation mode on an orbit beginning with an eclipse and full battery capacity. This timeline ensures that the power margin obtained in the power budget is actually used to charge the battery.
With a charging current of 130mA, it can be seen that the battery is charged again after 37 minutes 32 seconds.
During the final minutes of the orbit, the BCR is no longer activated and the power harvest of the solar cells is only limited by the power consumption of teh satellite.

The second timeline represents the transmission operation mode for 6 minutes and 12 seconds. In this scenario, the transmission is used twice during the sunlight period of the orbit. The DoD of the battery at the beginning of the orbit is 93.6%, the DoD at the end of an eclipse.

The battery can be charged when no transmissions are activated.
As the power consumed during the transmissions is higher than the power harvested, the battery is connected to the bus and start discharging.
It can be seen that the period without transmission are enough to fully charge the battery.

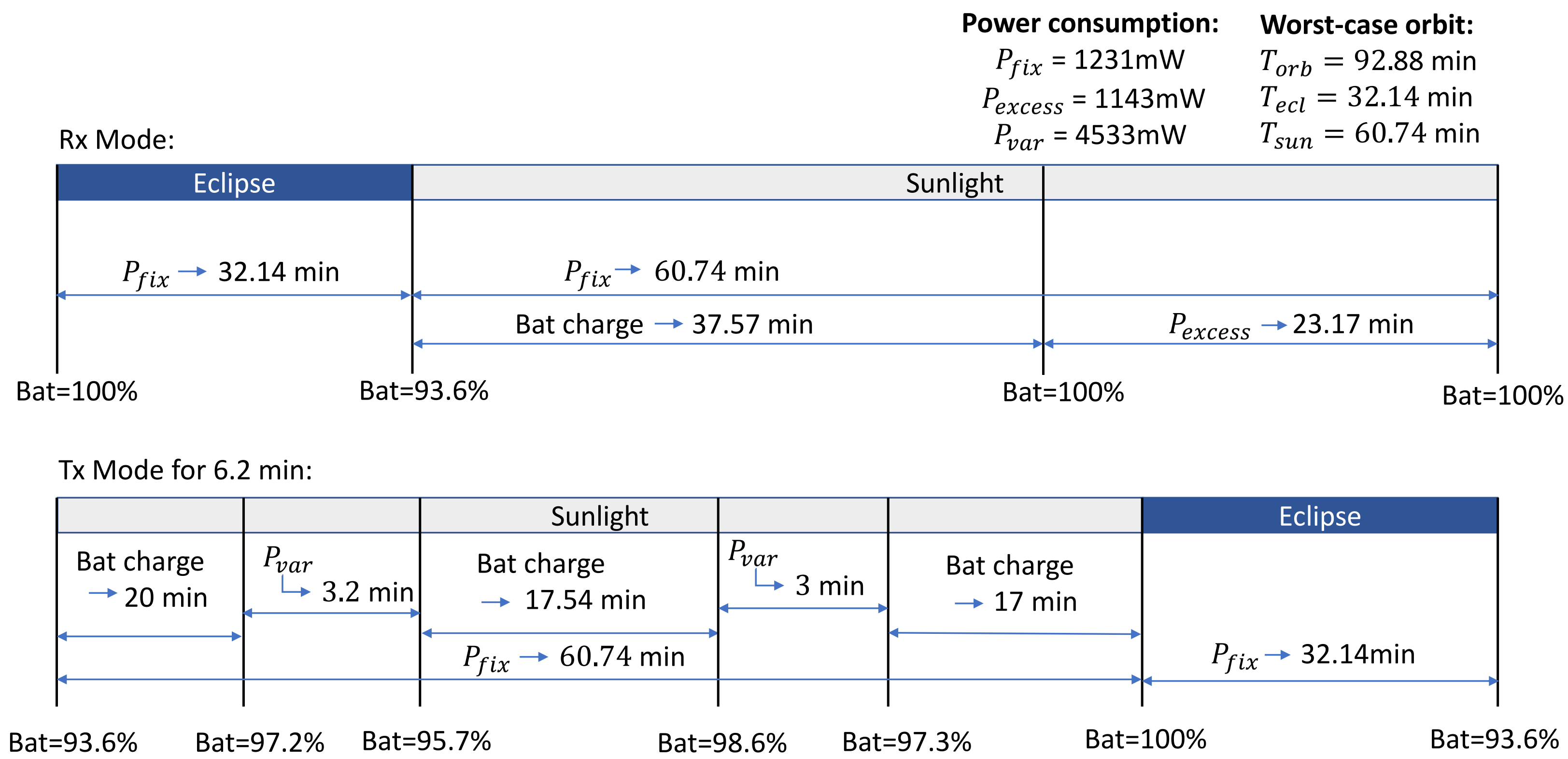

Figure 10.3: Timeline of the Depth of Discharge of the battery over a worst case orbit, for a receiver mode only scenario and for transmission mode of 6.2 minutes scenario

10.3 Conclusion

This section has ensured that the EPS design fits the use of the D-STAR payload. Enough power is ensured to supply the sub-systems and to charge the battery during the standard mode orbit.

A charging current of 130mA is chosen to charge the battery with a MCP73213 BCR. Up to 3.6% of net charge over an orbit in the worst case scenario can be achieved when no transmissions are operated.

Transmissions up to 6 minutes and 12 seconds in a worst case orbit can be operated without affecting the state of the battery over an orbit.
Longer communications can be established, even though the battery is depleted. This discharge is acceptable as long as the DoD of the battery does not exceed 20%. Standard operation mode orbits are then needed to recharge the battery.

11 Live Experience and further work

11.1 Spanish Small Satellite International Forum (SSSIF)

I had the chance to present OUFTI-2 at the SSSIF event. I warmly thank Mr Valery Broun and Mr Jacques Verly that offered me this opportunity.

The poster I designed with the help of Mr Verly and Mr Broun is in the appendix. This poster gathers the main information about OUFTI-2, the high level architecture of its EPS and a brief review of the power budget philosophy.
As this event took place 7$^{\text{th}}$ and 8$^{\text{th}}$ March 2019, at the beginning of my thesis, the results presented were not the final one.
I could talk with several professors and students about the nanosatellites they implemented and their respective EPS, among which UPM SAT 2 from the Polytechnical University of Madrid.

This rich experience brought me some knowledge about the *space* field. I discovered the "new space" market through presentation made by Mr Andreas Martinez, NASA representative and Jordi Puig-Suari, professor at CalPoly University and inventor of the CubeSat concept.
This market is flourishing and will sure play an important role in a near future.
This experience also broaden my network through many contacts with space industries.

11.2 Further work

Now that an architecture design is pointed out. In order to test the engineering model of the finalised EPS board of OUFTI-2, several works have yet to be done:

- Measure of the power harvested by the design with several spectrolab solar panels
- Test of the four DC/DC converters TPS62130 on the actual EPS board
- Design and implementation of the engineering model of the EPS board on PC104 format
- Test of the EPS engineering model on its own
- Test of the EPS engineering model with all the sub-systems
- Comparison of the estimated power budget with the actual consumptions of all sub-systems

12 Conclusion

This thesis discussed and compared four different architecture designs of power harvesting and management systems of the Electronic Power Supply (EPS) board of the nanosatellite OUFTI-2.
The requirements of the `Spectrolab` solar panels and the `clydespace` battery pack are analysed and it is shown that the use of Maximum Power Point Tracking (MPPT) controllers and a Battery Charger (BCR) are necessary.
Scripts that simulate the current versus voltage (I-V) curve of a 26.62 cm^2 `spectrolab` UTJ solar cell were adapted in order to understand its behaviour and estimate its Maximum Power Point (MPP) under different conditions.

A state of the art of the MPPT algorithms, as well as a non-exhaustive review of the cubesat EPS pointed out the SPV1040 chip implementing the Perturb & Observe (P&O) algorithm as MPPT controller. This chip is reliable, efficient and has flight heritage.

From these conditions it is shown that a semi-regulated bus is required to decouple the MPPT controllers and the battery.

The Constant Current / Constant Voltage (CCCV) charging method and the principle of linear and switching mode BCR for Lithium Polymer (LiPo) battery cells are summarised.
Even though a linear BCR is less efficient than a switch-mode BCR, the low complexity of the linear charger makes it way more reliable, a serious advantage for critical space application.

Several architectures are compared: A parallel connection of 5 MPPT controllers in cascade with a boost BCR and a series connection of 2, 3 and 5 MPPT controllers followed by a linear BCR.
The parallel and series configurations of the SPV1040 MMPT controllers are tested. The output voltage of both configuration as well as their efficiency are measured and stored in a comparison table.
Based on this table, the architecture chosen for the power management and harvesting systems of the EPS of OUFTI-2 is the design of two SPV1040 MPPT controllers in series followed by a MCP73213 linear BCR.
This architecture is chosen for its high reliability, low voltage bus and good efficiency.

The power path of this solution regulates the bus voltage to 9.8V when the two SPV1040 controllers produce more power than the power consumed. When more power is consumed by the satellite than the power harvested by its solar panels, the voltage of the bus drops to the battery voltage, and the latter discharges in the semi-regulated bus.

Finally the power budget of the satellite is established to estimate the power consumption of the sub-systems according to different operation of the satellite.
This consumption is then compared to the harvested power in a worst case scenario: an orbit with an eclipse duration of 32.14 minutes.
This analysis ensures the battery to recharge and the satellite to be supplied.
It is shown that the power harvested can be used to operate the D-STAR payload and the control transmissions for 6 minutes and 12 seconds per orbit during light-time.
Longer transmissions can also be operated with the help of the battery up to a DoD of 20%.
However, no transmission must be operated in the 6 next orbits to fully recharge the battery.

On a personal point of view, this thesis was a rich and unforgettable experience allowing me to get hands-on on a real space application project. I could learn to use `Altium Designer` and `STK` programs. I also learned to solder surface mounted design components and implement my own PCB. These new skills will for sure be useful for many other projects.

Bibliography

[1] NASA CubeSat Overview.
https://www.nasa.gov/mission_pages/cubesats/overview.
Accessed: 2019-02-28.

[2] OUFTI-1 project description.
http://www.leodium.ulg.ac.be/cmsms/index.php?page=home.
Accessed: 2019-02-28.

[3] V. Beukelaers.
From mission analysis to space flight simulation of the oufti-1 nanosatellite.
Master's thesis, University of Liège, 2008-2009.

[4] GKToday, General studies: Earth's Magnetosphere.
https://www.nasa.gov/mission_pages/cubesats/overview.
Accessed: 2019-03-9.

[5] P. Thirion.
Design and implementation of on-board electrical power supply of nanosatellite oufti-1.
Master's thesis, University of Liège, 2008-2009.

[6] V. Francois-Lavet.
Study of passive and active attitude control systems for the oufti nanosatellites.
Master's thesis, University of Liège, 2009-2010.

[7] Spectrolab: 28.3% Ultra Triple Junction Solar Cells, 2012.
Datasheet-2012.

[8] Edgars Pavlovskis on behalf of Clydespace.
User manual: 3rd generation cubesat battery family.

[9] J. Jeevarajan.
Pc104 consortium.
https://pc104.org/consortium/history/.
Accessed: 2019-02-28.

[10] Eduardo Lorenzo.
Solar electricity: Engineering of photovoltaic systems - 1994.

[11] Fabrice Frebel.
Lecture notes 1: Elements of Power Electronics - ELEC0055.
Faculty of Applied Sciences of the University of Liège, December 2018.

[12] Ahmed. F. Zobaa Ramdan B. A. Koad.
Comparative study of five maximum power point tracking techniques for photovoltaic systems, *Brunel University of London.*

[13] D. P. Hohm and M. E. Ropp.
Comparative study of maximum power point tracking algorithms.
IEEEexplore, pages 47–62, 2003.

[14] N. Onat.
Comparative study of mppt algorithm.
`https://www.hindawi.com/journals/ijp/2010/245316/`.
Marmara University of Istanbul.

[15] STelectronics Inc.
High efficiency solar battery charger with embedded mppt, 2017.
SPV1040 datasheet.

[16] M. Chessab Mahdi ans J. Sadiq.
Design and implementation of an effective electrical power system for nano- satellite.
Master's thesis, Al-Furat Al-Awsat Technical University, 2014.

[17] J. Hemmo.
Electrical power systems for finnish nanosatellites.
Master's thesis, Aalto University, 2013.

[18] James E. Lumpp Jr. Samuel F. Hishmeh, Tyler J. Doering.
Design of flight software for the kysat cubesat bus.
Master's thesis, University of Kentucky, 2008.

[19] F. Gudmundsson C. Kejser T. Koustrup C. Lodberg T. Viscor L. Alminde, M. Bisgaard.
Power supply unit for the aau-cubesat, 2001.
Aalborg University.

[20] L. E. Jacobsen.
Power system of the ntnu test satellite backplane study and design of the eps.
Master's thesis, Norwegian University of Science and Technology, 2011.

[21] K. Olav Skyttemyr.
Design and implementation of the electrical power system for the cubestar satellite.
Master's thesis, University of Oslo, 2012-2013.

[22] STelectronics inc.
Solar battery charger using the spv1040, application note, 2017.
STEVAL-ISV006V2 datasheet.

[23] A. Guiseppi-Elie J. M. Amanor-Boadu and E. Sánchez-Sinencio.
The impact of pulse charging parameters on the life cycle of lithium-ion polymer batteries.
Energy open access journals, page 2, 2018.

[24] Texas Instrument.
3v to 17v, 3a step-down converter, 2016.
TPS62130 datasheet.

[25] Poly-crystalline Epoxy Solar Panel.
SZGD7050-3P Datasheet.

[26] Y. Kushnir.
Solar radiation and the earth's energy balance lecture, columbia university.
https://eesc.columbia.edu/courses/ees/climate/lectures/radiation/index.html.
Accessed: 2019-04-28.

[27] Linear Technology.
Ltc4110-battery backup system manager, 2017.
LTC4110 datasheet.

[28] Analog Electronics.
Quick start guide for demonstration circuit dc1259a: Battery backup manager board.
DC1259A datasheet.

[29] Microchip.
Mcp73213: Dual-cell li-ion / li-polymer battery charge management controller with input overvoltage protection, 2009.
MCP73213 datasheet.

[30] ISS: International Space Station .
https://www.esa.int/Our_Activities/Human_and_Robotic_Exploration/International_Space_Station/ISS_International_Space_Station.
Accessed: 2018-11-12.

Appendix

Solar Cell Models codes

Cell_UJT.m

```
function I = Cell_UJT(V,G,TaC)
%Code produced by the team from the CubeSat SwissCube
%modified by Philippe Ledent (OUFTI-1)
%modified by Francois Grosjean (OUFTI-2)
%
%Model of 28% efficiency solar cell from Spectrolab : I=f(V,T)
%Use of function : I = Cell_GaAs(V,G,TaC)
%V = Voltage on cell terminals [V]
%G = relative insolation [-] (G=1 => 1367 W/m^2)
%TaC = temperature of the cell in operation [Celsius]

%Boltzman constant
k = 1.38e-23;
%Electric charge
q = 1.60e-19;
%Quality factor of the diode (1<n<2)
n = 1.5;
%Band gap voltage (1.12eV < Vg < 1.757eV)
Vg = 1.75;
%Reference values
A=26.62;%Area of the cell [cm2]
 Tref = 273 + 28; %temperature
 Voc_Tref = 2.660; %open circuit voltage (G=1 et T=Tref)
 Isc_Tref = 17.05*A/1000; %short circuit current (G=1 et T=Tref)[A]
%Temperature of the cell in operation
TaK = 273 + TaC;
%Photo-current thermal coefficient
K0 = 2.72e-4/Isc_Tref;
%Photo-current (G=1 et T=Tref)
Iph = Isc_Tref * G * (1 + K0*(TaK - Tref));
%Diode saturation current (T=Tref)
Id_Tref = Isc_Tref / (exp(q*Voc_Tref/(n*k*Tref))-1);
```

```
%Diode saturation current (T=Tak)
Id = Id_Tref * (TaK/Tref)^(3/n) * exp(-(Vg * q/(n*k))*(1/TaK - 1/
    Tref));
%Calculation of serie resistance Rs
Vpmax_Tref = 2.350; %voltage at maximum power for T=Tref
Ipmax_Tref = 16.3*A/1000; %current at maximum power for T=Tref
Rs = (Voc_Tref-Vpmax_Tref)/Ipmax_Tref;
%Iterative calculation of Isc
I = zeros(size(V));
for i=1:10 %number of iteration = 10
    for j=1:length(V)
        I(j) = I(j) - (Iph - I(j) - Id*(exp(q*(V(j)+I(j)*Rs)/(n*k*
            Tref)) -1))/...
             (-1 - (Id*(exp(q*(V(j)+I(j)*Rs)/(n*k*Tref)) -1))*q*Rs/(n
                *k*Tref));
    end
end
```

plotcell.m

```
% Script implemented by Francois Grosjean (OUFTI-2)
% Different plots of the IV characteristic of a 26.64 cm^2 UTJ cell

function plotCell(G,TaC)
%close all
% Plots the IV characteristic of a solar panel of OUFTI-2
% i.e. two solar cells of 23.64 cm^2 in series

vmax=3;% Maximum voltage of the curve
%Resolution of the curve :
V=0:0.005:vmax;
I = Cell_UJT(V,G,TaC);
Imax=max(I);
P=V.*I;
Pmax=max(P);

figure
V=2.*V;
P=V.*I;
```

```
[Pmax, Index]=max(P);
VMPP=V(Index);

str = sprintf('in series at %dC and under a %1.1f W/m^2 insolation',
    TaC, G*1367);
title({'I-V and P-V curves of two 26.62 cm^2 Spectrolab UTJ cells',
    str})
grid on
yyaxis left
plot(V,I,'-b')
ylim([0 1.5*Imax])
ylabel('Current [A]')
yyaxis right
plot(V,P)
ylim([0 1.1*Pmax])
ylabel('Power [W]')
xlim([0 2*vmax])
xlabel('Voltage [V]')

end
```

load2.m

```
% Script implemented by Francois Grosjean (OUFTI-2)
% Plot the solar cell characteristic with the intersection of
    certain loads
function load2(G,TaC)
close all
vmax=3;% Maximum voltage of the curve
%Resolution of the curve :
V=0:0.005:vmax;
I = Cell_UJT(V,G,TaC);
V=2.*V;
P=V.*I;
R=[5,10,25];%ohm
for i=1:length(R)
    Ir(i,:)=V/R(i);
end
figure
```

```
grid on
plot(V,I,'-b')
ylim([0 0.7])
ylabel('Current [A]')
xlim([0 2*vmax])
xlabel('Voltage [V]')
for i=1:length(R)
    hold on
    plot(V,Ir(i,:))
    xlim([0 2*vmax])
end
grid on
legend('Solar panel''s IV curve', 'R=5 Ohm','R=10 Ohm ','R=25 Ohm')
str = sprintf('at %dC and under a %1.1f W/m^2 insolation', TaC, G*1367);
title({'I-V curves of two 26.62 cm^2 Spectrolab UTJ cells in series and various loads ',str})
end
```

plotCellsG.m

```
% Script implemented by Francois Grosjean (OUFTI-2)
% Different plots of the IV characteristic of two 26.64 cm^2 UTJ cells
% Four relative insolations G are compared
close all
vmax=3;% Maximum voltage of the curve
%G = relative insolation [-] (G=1 => 1367 W/m^2)
%TaC = temperature of the cell in operation [Celsius]

G=[0.7,0.8,0.9,1];

TaC=28;
Voc=zeros(1,4);
VMPP=zeros(1,4);
Imax=zeros(1,4);
Pmax=zeros(1,4);
figure
grid on
```

```
for i=1:4
    V=0:0.005:vmax;
    I = Cell_UJT(V,G(i),TaC);
    I(I<0) = 0;
    idx = find(I==0, 1, 'first');
    V=2.*V;
    P=V.*I;
    Voc(i)=V(idx);
    Imax(i)=max(I);
    % Plots the IV characteristic of a solar panel of OUFTI-2
    % i.e. two solar cells of 23.64 cm^2 in series
    [Pmax(i),index(i)]=max(P);
    VMPP(i)=V(index(i));
    plot(V,P)
    ylim([0 1.1*Pmax(i)])
    ylabel('Power [W]')
    xlim([0 2*vmax])
    xlabel('Voltage [V]')
    hold on
    K(i)=VMPP(i)./Voc(i);
end
```

plotCellsT.m

```
% Script implemented by Francois Grosjean (OUFTI-2)
% Different plots of the IV characteristic of two 26.64 cm^2 UTJ cells
% Four temperatures TaC are compared under a relative insolation G=1

close all
vmax=3;% Maximum voltage of the curve
%G = relative insolation [-] (G=1 => 1367 W/m^2)
%TaC = temperature of the cell in operation [Celsius]
TaC=[-10,0,20,55];
G=1;
Voc=zeros(1,4);
VMPP=zeros(1,4);
Imax=zeros(1,4);
Pmax=zeros(1,4);
```

```
figure
grid on
for i=1:4
    V=0:0.005:vmax;
    I = Cell_UJT(V,G,TaC(i));
    I(I<0) = 0;
    idx = find(I==0, 1, 'first');
    V=2.*V;
    P=V.*I;
    Voc(i)=V(idx);
    Imax(i)=max(I);
    % Plots the IV characteristic of a solar panel of OUFTI-2
    % i.e. two solar cells of 23.64 cm^2 in series
    [Pmax(i),index(i)]=max(P);
    VMPP(i)=V(index(i));
    plot(V,P)
    ylim([0 1.3*Pmax(i)])
    ylabel('Power [W]')
    xlim([0 2*vmax])
    xlabel('Voltage [V]')
    hold on
    K(i)=VMPP(i)./Voc(i);
end
```

Aeff_calc.m

```
% Script to import data from STK and compute the effective area on an
% orbit
[num,txt,raw] = xlsread('Aeff.xlsx');
Aeffs=num(3017:end,1);
Aeffs(Aeffs==0) = [];
mean(Aeffs)
```

STK ancillary (.anc) files to simulate OUFTI-2

```
<?xml version = "1.0" standalone = "yes"?>
<ancillary_model_data version = "1.0">
ARTICULATIONS:
```

```
Articulations are components (e.g., rocket stages, landing gear, doors,
and propellers) that move in various
ways. The motion is controlled via an articulation script.


POINTABLE ELEMENTS:
Pointable elements are components (e.g., radio dishes, cameras, and sun
tracking panels) that can
automatically point to and target other objects.
    <pointing_data>
        <pointing node = "ID50" vector = "0 0 1" />
    </pointing_data>


SOLAR PANEL GROUPS:
Solar Panel Groups are components defined as solar panels and assigned an
efficiency value. This is useful when running the STK solar panel tool.
    <solar_panel_groups>
            <solar_panel_group efficiency = "28" name = "SolaPanelYplus">
        <assigned_nodes>
            ID14
        </assigned_nodes>
    </solar_panel_group>
            <solar_panel_group efficiency = "28" name = "SolaPanelZplus">
        <assigned_nodes>
            ID37
        </assigned_nodes>
    </solar_panel_group>
            <solar_panel_group efficiency = "28" name = "SolaPanelZmoins">
        <assigned_nodes>
            ID51
```

```
                </assigned_nodes>
            </solar_panel_group>
                    <solar_panel_group efficiency = "28" name = "SolaPanelXplus">
                <assigned_nodes>
                    ID59
                </assigned_nodes>
            </solar_panel_group>
                    <solar_panel_group efficiency = "28" name = "SolaPanelXmoins">
                <assigned_nodes>
                    ID70
                </assigned_nodes>
            </solar_panel_group>
        </solar_panel_groups>

</ancillary_model_data>
```

Power Budget Excel Sheet

Power harvested

Power harvested estimation based on a worst case orbit and a mean insolation scenario.

Power harvested				
Tsun [min]	**Nbol [%]**	**Aeff mean [cm^2]**	**Nmppt [%]**	**Csunmean [W/m^2]**
92.88	28.3	66.37	92.5	1367
Worst case orbit:	**Teclipse [min]**	**%Sun**	**Pinst [mW]**	**Porb [mW]**
	32.14	65	**2375**	**1553**
Best case orbit:	**Teclipse [min]**	**%Sun**	**Pinst [mW]**	**Porb [mW]**
	24.8	73	**2375**	**1741**

Power consumption of a standard operation mode

Power consumed by different scenarii					
	Peak [mW]	Peak time [min]	Peak time [%]	Average [mW]	Percent of total [%]
AX.25 RX	163	92.88	100	163	**10.5**
AX.25 TX	4533	0	0	0	**0.0**
D-STAR	4533	0	0	0	**0.0**
BCN	88	46.44	50	44	**2.8**
BCN BURST	604	46.44	50	302	**19.5**
OBC/DPC	458	92.88	100	458	**29.5**
THER CST	110	92.88	100	110	**7.1**
THER + HEATER	220	32.14	35	76	**4.9**
RAD	18	92.88	100	18	**1.2**
IMU	18	92.88	100	18	**1.2**
Tx LOSS	345	0.0	0	0	**0.0**
CST LOSS	41	92.88	100	41	**2.7**
Total allocated				**1231**	**79.2**
Margin				322	**20.8**
Total power				**1553**	100.0

Power consumption of each sub-system				
Vbus	9.8		Ndcdc	0.91
	Voltage [V]	Current [mA]	System's consumption [mW]	Real consumption [mW]
BCN	5	16	80	88
BCN BURST	5	110	550	604
AX.25 RX	3.3	45	148.5	163
AX.25 - D-star TX	3.3	1250	4125	4533
THER CST	3.3	30	100	110
THER + HEATER	3.3	61	200	220
RAD	3.3	5	16.5	18
IMU	3.3	5	16.5	18
DPC				
Voltages [V]	**Current [mA]**	**Efficiency [/]**	**Real consumption [mW]**	**Total consumption**
3.3	50	0.91	181	**458**
1.8	126	0.82	277	

Power consumption when the transmissions are activated for 6.2min per orbit

Power consumed by different scenarii					
	Peak [mW]	Peak time [min]	Peak time [%]	Average [mW]	Percent of total [%]
AX.25 RX	163	92.88	100	163	**10.5**
AX.25 TX	4533	3.1	3	151	**9.7**
D-STAR	4533	3.1	3	151	**9.7**
BCN	88	46.44	50	44	**2.8**
BCN BURST	604	46.44	50	302	**19.5**
OBC/DPC	458	92.88	100	458	**29.5**
THER CST	110	92.88	100	110	**7.1**
THER + HEATER	220	32.14	35	76	**4.9**
RAD	18	92.88	100	18	**1.2**
IMU	18	92.88	100	18	**1.2**
Tx LOSS	345	6.2	7	23	**1.5**
CST LOSS	41	86.68	93	39	**2.5**
Total allocated				**1554**	**100.0**
Margin				0	**0.0**
Total power				**1553**	100.0

Power loss in the BUS

Bus losses

	Rx	Tx
Max Current drawn by the 3.3V DC/DC converter, [mA]	166	1340
Max Current drawn by the 5V DC/DC converter [mA]	110	110
Current drawn by the 1.8V DC/DC	126	126
Max BUS current, [mA]	151	586

		Diode A	Diode B		Reset	Current sensor	Fuse	Total loss [mW]
	Forward voltage [V]	0.24	0.24	Resistance [mΩ]	20	20	28	
Rx	Current through the diode [mA]	83	83	Current through the component [mA]	151	151	151	**41**
	Power loss [mW]	20	20	Power loss [mW]	0.5	0.5	0.6	
Tx	Current through the diode [mA]	670.2	670.2	Current through the diode [mA]	585.9	585.9	585.9	**345**
	Power loss [mW]	160.8	160.8	Power loss [mW]	6.9	6.9	9.6	

CAD layout

This section presents the schematics and PCB layout of the prototype board to test the MPPT controllers in series as well as the linear battery charger.

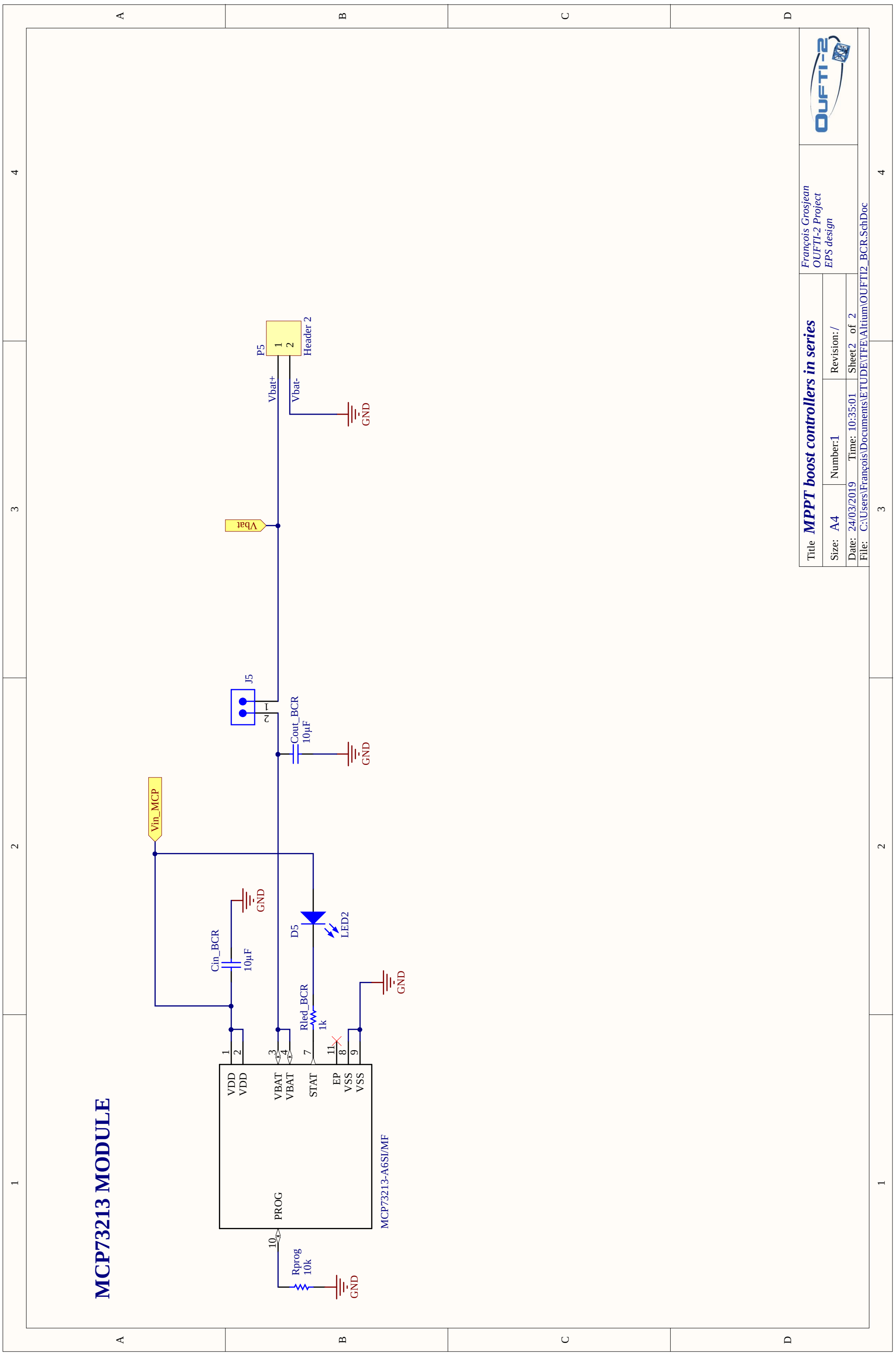
MCP73213 MODULE
MCP73213-A6SI/MF
VDD
VDD
VBAT
VBAT
STAT
EP
VSS
VSS
PROG
Rprog
10k
GND
Cin_BCR
10µF
Vin_MCP
D5
LED2
Rled_BCR
1k
Cout_BCR
10µF
J5
Vbat
Vbat+
Vbat-
P5
Header 2
Title
MPPT boost controllers in series
François Grosjean
OUFTI-2 Project
EPS design
Size: A4
Number:1
Revision:/
Date: 24/03/2019
Time: 10:35:01
Sheet2 of 2
File: C:\Users\François\Documents\ETUDE\TFE\Altium\OUFTI2_BCR.SchDoc

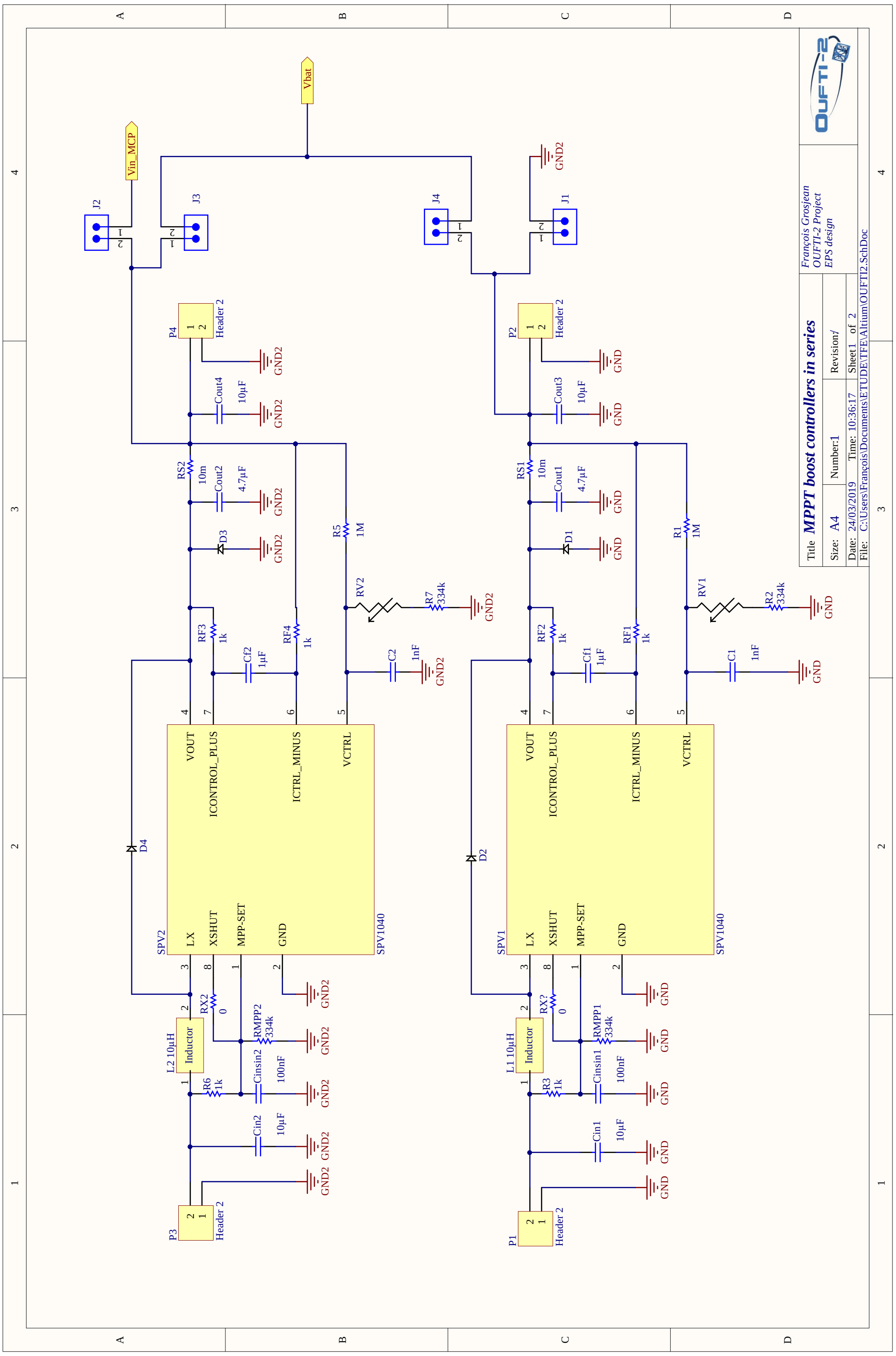
MPPT boost controllers in series
François Grosjean
OUFTI-2 Project
EPS design
Size: A4
Number:1
Revision:/
Date: 24/03/2019
Time: 10:36:17
Sheet1 of 2
File: C:\Users\François\Documents\ETUDE\TFE\Altium\OUFTI2.SchDoc
SPV1040
SPV1
SPV2
VOUT
ICONTROL_PLUS
ICTRL_MINUS
VCTRL
LX
XSHUT
MPP-SET
GND
Vbat
Vin_MCP
GND2

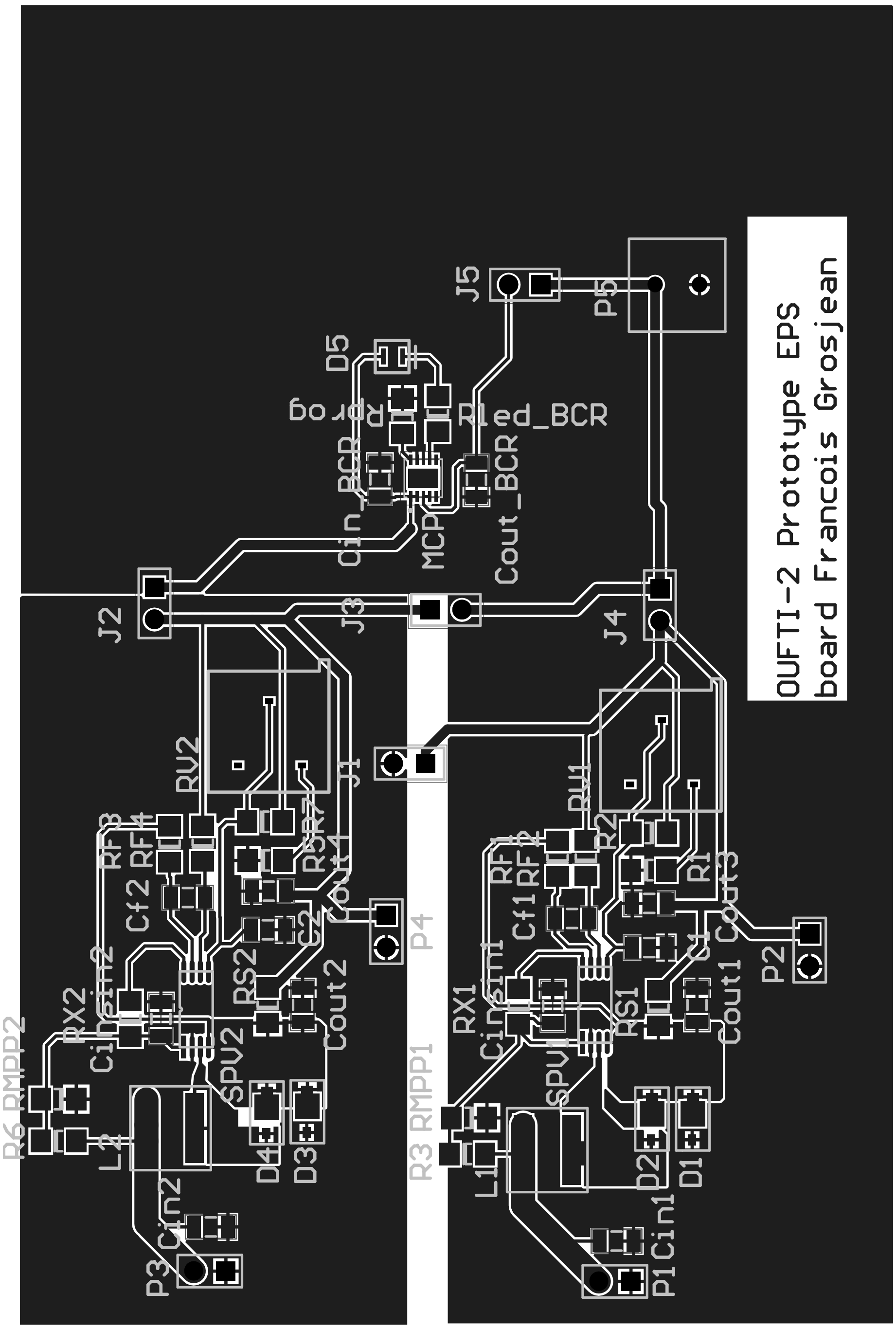
OUFTI-2 Prototype EPS
board Francois Grosjean

SSSIF: poster

SPANISH SMALL SATELLITES INTERNATIONAL FORUM
#SSSIF2019
7-8 March, 2019
Málaga (Spain)

OUFTI-2 LIÈGE université HEPL Haute Ecole de la Province de Liège

Architecture of the electrical power supply (EPS) of the new CubeSat OUFTI-2

1. OUFTI-2

- Educational 1-U CubeSat
- Payloads:
  - D-STAR radiocommunication repeater
  - Test of efficiency of new shield against space radiation
  - Thales Alenia Space DPC as OBC
- ISS deployment:
  - Lifetime < 1 year
- ClydeSpace LiPo batteries
  - Nominal voltage of 7.6V
  - Nominal capacity of 1300mAh
  - Protection features
  - Compatible with ISS manned flight
- Spectrolab solar cells
  - Ultra-Triple-Junction
  - 28.3% BOL efficiency
  - $A = 26.62\text{cm}^2$ per cell
  - $J_{sc} = 17.05\text{mA}/\text{cm}^2$ per cell

2. Exploded view

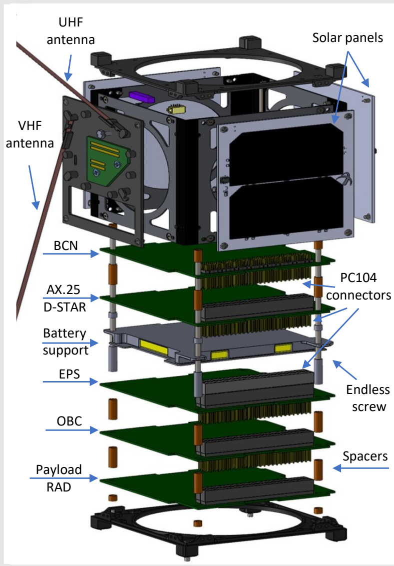

OBC = On-board computer
BCN = Beacon
EPS = Electrical power supply

3. MPPT

MPPT SPV1040

- Low power
- Step-up converter
- Perturb & observe MPPT algorithm
- Up to 95% efficiency

4. Battery charger

BCR MCP73213

- Dual LiPo cells charger
- Specific CC/CV charge algorithm
- [4-16]V input range
- Protection features

5. Power budget

Computations based on a time interval of one orbit

Mean input power:

$$P_{in} = \eta_{mppt}\eta_{pv}A_{eff}C_{mean} = 1589\text{mW}$$

vs

Power consumed by different operation modes:

$$P_{cons} = \sum_i T_i(\%)P_{sub,i}$$

1. Standard mode:
All sub-systems activated except for D-STAR & AX.25 TX
$P_{cons} = 1134\text{mW}$
Net power margin of 455mW

2. Tx mode:
Additional D-STAR activation during 10% of the orbit
$P_{cons} = 1589\text{mW}$
No net power margin

A_{eff} = Effective area of all solar cells [m^2]
C_{mean} = Mean solar constant [W/m^2]
T_i = Duration of activation of sub-system i [%]
$P_{sub,i}$ = Power consumed by sub-system i [W]

6. High-level EPS architecture

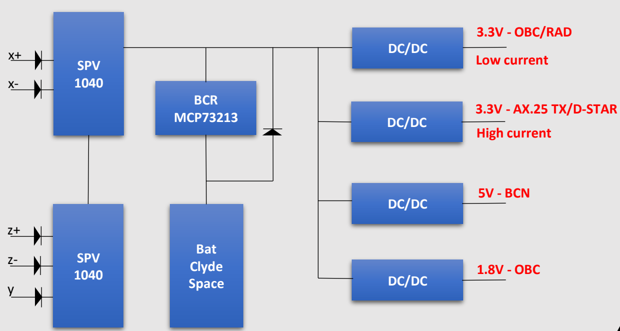

Contact data

AUTHORS:
François Grosjean, Jacques Verly; Dept. of Electrical Engineering & Computer Science, University of Liège, Belgium;
Valery Broun, Sebastien De Dijcker; Engineering Dept., HEPL, Belgium
E-mail: francois.grosjean@student.uliege.be